Inorganic Chemistry

pubs.acs.org/IC Article

Electrochemical Detection of a Novel Pt(IV) Prodrug with the Metronidazole Axial Ligand in the Hypoxic Area

Daniil V. Spector, Alexander S. Erofeev, Petr V. Gorelkin, Alexander N. Vaneev, Roman A. Akasov, Nikolay V. Ul'yanovskiy, Vita N. Nikitina, Alevtina S. Semkina, Kseniya Yu Vlasova, Mikhail A. Soldatov, Alexander L. Trigub, Dmitry A. Skvortsov, Alexander V. Finko, Nikolay V. Zyk, Dmitry A. Sakharov, Alexander G. Majouga, Elena K. Beloglazkina, and Olga O. Krasnovskaya*

Cite This: *Inorg. Chem.* 2022, 61, 14705−14717 Read Online

ACCESS | Metrics & More | Article Recommendations | Supporting Information

ABSTRACT: We report herein a Pt(IV) prodrug with metronidazole in axial positions **Pt-Mnz**. The nitroaromatic axial ligand was conjugated with a cisplatin scaffold to irreversibly reduce under hypoxic conditions, thereby retaining the Pt(IV) prodrug in the area of hypoxia. X-ray near-edge adsorption spectroscopy (XANES) on dried drug-preincubated tumor cell samples revealed a gradual release of cisplatin from the **Pt-Mnz** prodrug instead of rapid intracellular degradation. The ability of the prodrug to penetrate into three-dimensional (3D) spheroid cellular cultures was evaluated by a novel electrochemical assay via a platinum-coated carbon nanoelectrode, capable of single-cell measurements. Using a unique technique of electrochemical measurements in single tumor spheroids, we were able to both detect the real-time response of the axial ligand to hypoxia and establish the depth of penetration of the drug into the tumor model.

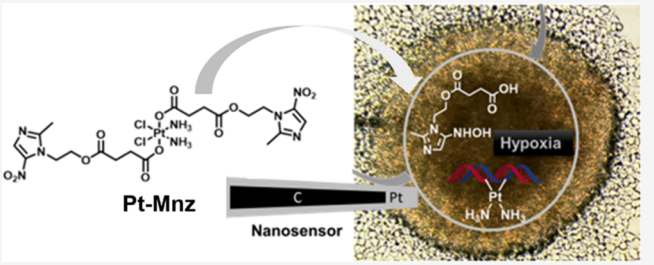

INTRODUCTION

Although platinum(II)-based chemotherapy is extremely important in the treatment of malignant tumors,[1] Pt(II) complexes are prone to nonselective ligand exchange with an estimated approximately 90% of the administered cisplatin being deactivated in the bloodstream by irreversible binding to plasma proteins.[2] This results in only 1% (or less) binding of the administrated Pt(II) to its intended target, the nuclear DNA.[3] To overcome the drawbacks of Pt(II)-based therapy, Pt(IV) complexes with low-spin d6 octahedral geometry, which are supposed to exhibit kinetic inertness, have been designed.[4−8] Despite the evident benefits of Pt(IV) complexes, their clinical use is limited due to their fast reduction in the bloodstream and resulting from this low efficacy in vivo.[9−15] Concerns are also raised regarding the hydrolytic stability of Pt(IV) prodrugs at physiological pH.[16−18] Therefore, developing kinetically inert Pt(IV) prodrugs capable of slowly releasing cisplatin is of interest.

Solid tumors are poorly vascularized, which results in forming drug-insensitive hypoxia regions.[19] Hypoxia, a decreased supply of oxygen in tissues, is a key biomarker of solid tumors and is also considered a major factor of tumor resistance to chemotherapy.[20] Hypoxia can influence the cell resistance to drug therapy by various methods, including the formation of specific cell populations, e.g., tumor-associated fibroblasts and stem cells.[21] Although targeting hypoxic areas of solid tumors is a relevant task, only a few hypoxia-sensitive Pt(IV) prodrugs basically targeting the intricacies of the hypoxic cell metabolism have been reported.[22,23] Pt(IV) prodrugs capable of targeting hypoxia-inducible factor-1α (HIF-1α) have been reported, namely, cisplatin and oxoplatin conjugate with the HIF-1α inhibitor YC-1 (1-benzyl-3-(5-hydroxymethyl-2-furyl)indazole),[24] or clofibric acid, capable of decreasing the HIF-1α level.[25] Also, Pt(IV) prodrugs with carbonic anhydrase IX (CAIX) inhibitors, which are mediators of hypoxia-induced stress, are reported.[26]

A variety of methods to assess the degree of hypoxia in solid tumors have been reported, including oxygen-sensitive electrode measurements,[27] immunohistological staining,[28] and small-molecule-based hypoxia markers. Nitroimidazole derivatives are commonly used hypoxia markers. [^{18}F]-Fluoromisonidazole ([^{18}F]FMISO)[29] is a PET-hypoxia-imaging agent for the visualization of poorly oxygenated regions;[30] pimonidazole[31] is a hypoxia detection agent. These hypoxia-imaging agents are able to bind covalently with cellular macromolecules when the level of oxygen is lower than 1.3%. A

Received: June 14, 2022
Published: September 1, 2022

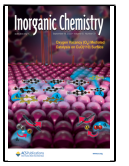

https://doi.org/10.1021/acs.inorgchem.2c02062
Inorg. Chem. 2022, 61, 14705−14717

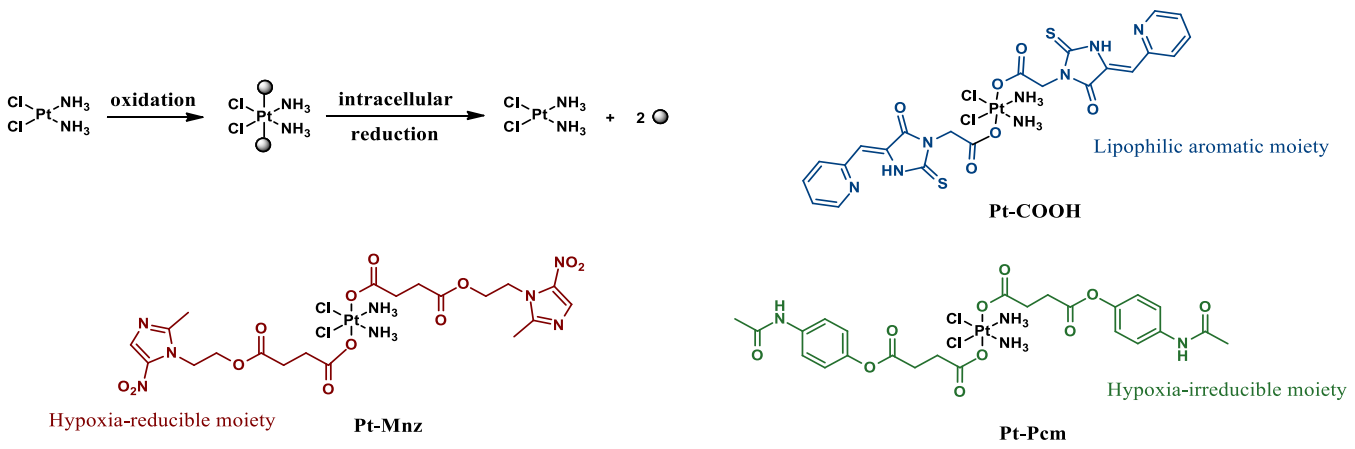

Figure 1. Platinum(IV) prodrugs with hypoxia-sensitive axial ligands **Pt-Mnz**, and reference compounds **Pt-COOH** and **Pt-Pcm**.

Table 1. Inhibition of Cell Proliferation by Pt-Mnz, Pt-COOH, and Pt-Pcm in Human Embryonic Kidney (HEK-293T), Human Breast Adenocarcinoma (MCF-7), Human Lung Adenocarcinoma (A-549), and Human Embryonic Lung (Va13) Cell Lines Determined by the MTT Assay after 72 h of Incubation

		cell line, IC_{50} value [μM][a]			
compound	*A* log *P*[a]	HEK-293T	MCF-7	A-549	Va13
Pt-Mnz	2.49	7.7 ± 0.6	6.6 ± 0.6	11.6 ± 1.4	13.5 ± 1.1
Pt-Pcm	3.38	15.1 ± 7.2	50.2 ± 7.4	~120	19.7 ± 1.3
Pt-COOH	3.29	10.2 ± 5.0	4.5 ± 2.0	13.0 ± 4.3	4.0 ± 1.3
cisplatin		11.8 ± 0.8	10.9 ± 1.5	6.5 ± 0.5	3.7 ± 0.3

[a]Calculated using www.vcclab.org.

significant correlation between the hypoxia level and the intensity of intracellular binding of the 2-nitroimidazole derivatives was established in vitro and in vivo.[32] Metronidazole is an FDA-approved well-known pharmacophore for treating a broad range of parasites. Due to its anaerobic reduction ability, metronidazole is recognized as the "gold standard" in the treatment of anaerobic infections.[33−35] Metronidazole is also an inhibitor of aldehyde dehydrogenase and can increase the antiproliferative action of cisplatin in the hypoxic zone.[36] Herein, we designed a novel Pt(IV) prodrug, a twin cisplatin/metronidazole drug, in an attempt to design a prodrug with a hypoxia-reducible axial ligand, which can cause the drug to "get stuck" in the hypoxic area.

Nanopipette is a unique platform in single-cell chemistry.[37−40] Carbon nanoelectrodes (CNEs) are actively used for the measurement of reactive oxygen and nitrogen species (ROS/RNS) in single cells.[41−46] We had also previously detected ROS electrochemically at the single cell level[47−50] and in vivo[51] using Pt-coated CNEs (PtNEs). Recently, we had developed a PtNE-based technique able to quantify Pt(II) species in individual cells, cellular spheroids, tumors, and tissues in vivo.[52] More recently, we used the PtNE-based technique to evaluate the efficacy of various Pt(IV) prodrugs in a spheroid tumor model and in vivo.[53]

In the current research, we have applied the PtNE technique for real-time monitoring of the Pt(IV) prodrug metabolism in a hypoxic tumor model. The metronidazole moiety in the axial position should reduce under hypoxic conditions, thereby retaining the prodrug in the depth of the spheroid. To confirm this, we used electrochemical measurements in single tumor spheroids via the PtNE technique. Using this unique technique, we were able to both detect the real-time response of the axial ligand to hypoxia and establish the depth of penetration of the drug into the tumor model. To the best of our knowledge, for the first time, the hypoxia-induced Pt(IV) prodrug metabolism has been detected within a single tumor spheroid.

RESULTS AND DISCUSSION

Synthesis and Characterization of Pt(IV) Prodrugs. We designed a Pt(IV) prodrug **Pt-Mnz** by conjugating a succinate-bridged hypoxia-reducible metronidazole axial ligand onto a cisplatin scaffold. We also designed two model Pt(IV) prodrugs with nonreducible under hypoxic conditions axial ligands as reference drugs. A structurally similar Pt(IV) prodrug with the succinate-bridged COX-inhibitor paracetamol **Pt-Pcm** and the Pt(IV) prodrug with lipophilic moieties in axial positions **Pt-COOH** was synthetized and characterized (Figure 1 and Schemes S1−S3, Supporting Information). The reference drugs were designed as more lipophilic, while their axial ligands are unable to reduce under hypoxic conditions. log *P* values of Pt(IV) prodrugs were calculated using www.vcclab.org.

Cisplatin was oxidized according to Pathak et al.[54] Metronidazole and paracetamol were acylated by succinic anhydride following the literature procedures.[55,56] **Pt-Mnz** and **Pt-Pcm** were synthesized by activating the carboxylic group with HBTU and subsequent stirring with oxoplatin for 48 h. Organic ligands and Pt(IV) prodrugs were characterized by ^{1}H, ^{13}C, ^{195}Pt NMR, and HRMS spectra, and purity of the compounds was confirmed by HPLC data (Figures S1−S25, Supporting Information). Stability of the Pt(IV) prodrugs was confirmed using HPLC (Figures S28−S30 and Tables S1−S3, Supporting Information).

Electrochemical Study. The reduction of Pt(IV) prodrugs was assessed using cyclic voltammetry (Table S4 and Figures

https://doi.org/10.1021/acs.inorgchem.2c02062
Inorg. Chem. 2022, 61, 14705−14717

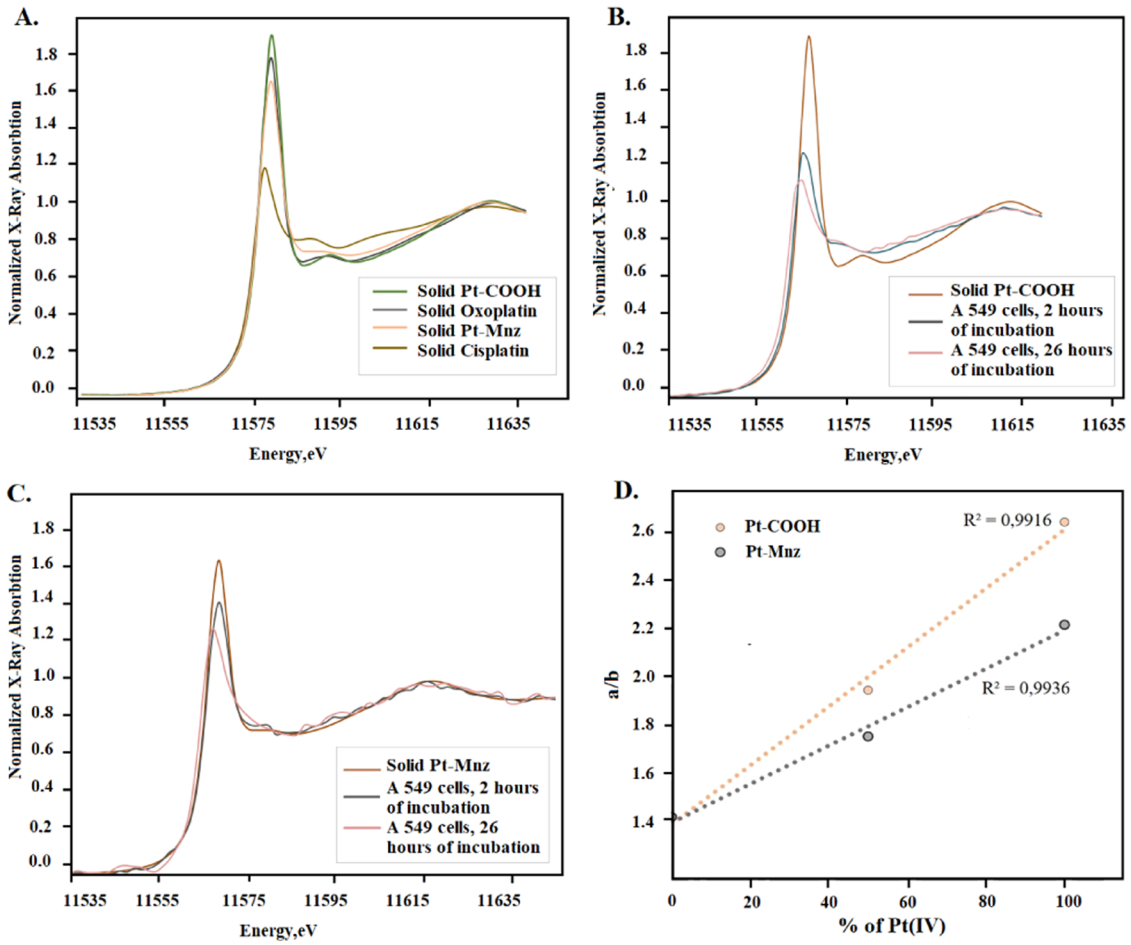

Figure 2. (A) Normalized XANES spectra of oxoplatin Pt(IV), **Pt-Mnz** Pt(IV), **Pt-COOH** Pt(IV), and cisplatin Pt(II). (B) Normalized XANES spectra of A549 cells incubated with **Pt-Mnz** (IV) for 2 and 26 h. (C) Normalized XANES spectra of A549 cells incubated with **Pt-COOH** (IV) for 2 and 26 h. (D) Linear approximation of the a/b parameter dependence from the ratio of the Pt(IV):Pt(II) mixture for samples of Pt(IV) prodrugs (100% of Pt(IV)), Cisplatin Pt(II) 0% of Pt(IV), and equimolar mixture Pt(II) + Pt(IV) 50:50.

S31−S33 Supporting Information). For **Pt-Mnz**, a reduction of the metronidazole moiety as well as Pt(IV) reduction should be observed. Thus, metronidazole was used as a control compound. A nitro-group reduction was observed at −1.5 V for both metronidazole and **Pt-Mnz** in a PBS:DMSO solution using the Ag/AgCl electrode. A Pt(IV) reduction was detected at ∼ −1 V, which is in good agreement with previous reports[57,58] (Figure S32, Supporting Information).

Square-wave voltammetry (SWV) was also used to evaluate a Pt(IV) reduction. A nitro-group reduction peak was detected at −1.26 V against ferrocene for both **Pt-Mnz** and metronidazole, and Pt(IV) reduction at −0.78 V was observed for **Pt-Mnz** (Figure S30, Supporting Information).

Cytotoxicity Assay. To evaluate the antiproliferative activity of synthesized Pt(IV) prodrugs against human cancer cells, we studied the cytotoxicity via an MTT assay on malignant cell lines, such as human breast adenocarcinoma (MCF-7), human lung adenocarcinoma (A-549), and non-tumor cell lines human embryonic kidney (HEK-293T) and human embryonic lung (Va13) (Table 1 and Figures S34−S36, Supporting Information). The IC_{50} values of **Pt-Mnz** in MCF-7 and HEK293 were higher than those of cisplatin; **Pt-COOH** showed comparable IC_{50} values. **Pt-Pcm** was drastically less toxic than cisplatin on all cell lines, so we used this prodrug only as a negative control, without a detailed examination of its intracellular metabolism.

Cellular Accumulation/Distribution. Intracellular accumulation of **Pt-Mnz** and **Pt-COOH** Pt(IV) prodrugs was studied using the ICP-MC assay (Figure S37 and Tables S5 and S6, Supporting Information). After 24 h of incubation, the cellular accumulation of **Pt-COOH** was comparable to that of cisplatin, mostly accumulating in the cytoplasm and nucleus. The intracellular platinum level for **Pt-Mnz** was 1.3-fold higher than for cisplatin. It is worth noting that almost two-third of platinum for **Pt-Mnz** accumulated in the nucleus and mitochondria, while only 27% cisplatin was found in those organelles. Despite the high lipophilicity of **Pt-COOH**, intracellular accumulation on the less lipophilic **Pt-Mnz** was higher. The importance of targeting mitochondria in cisplatin therapy is obvious, and designing a mitochondria-targeting Pt(IV) prodrug of cisplatin is relevant.[59−63]

Intracellular Metabolism Study Using XANES. X-ray near-edge adsorption spectroscopy (XANES) is a unique tool that makes it possible to estimate the ratio of compounds in Pt(IV)/Pt(II) oxidation states intracellularly.[64−72] For **Pt-Mnz** and **Pt-COOH** prodrugs, the intracellular metabolism was evaluated in accordance with the methodology developed by Hall et al.[64] XANES spectra of drug-preincubated dried tumor cells were registered. There is a linear correlation between the

https://doi.org/10.1021/acs.inorgchem.2c02062
Inorg. Chem. 2022, 61, 14705−14717

peak height ratio a/b of platinum L3 XANES spectra and the molar ratio of Pt(II)/Pt(IV), which allows one to study the reduction speed in various biological objects. Thus, we used the normalized white line height of XANES spectra of solid-state Pt(IV) prodrugs and cisplatin as well as dried A549 cells, incubated with **Pt-Mnz** or **Pt-COOH**, to quantitatively determine the Pt(II)/Pt(IV) ratio.

The peak height ratio a/b in the XANES spectra of L3 edge platinum is related linearly to the molar ratios of Pt(II)/Pt(IV), thus providing a tool for monitoring the reduction of Pt(IV) complexes in biological environments. Thus, the white line height of XANES spectra of Pt(IV) complexes, normalized to the post-edge minima, was used to quantitatively determine the proportion of each oxidation state in a Pt(II)/Pt(IV) mixture.

The XANES spectra of solid-state **Pt-Mnz** and **Pt-COOH** samples, oxoplatin, and cisplatin are shown in Figure 2; the obtained a/b values correlate with the previously published data for Pt(IV) prodrugs (Table 2).[68] Then, XANES spectra of dried tumor A-549 cell samples, preincubated for 2 and 26 h with **Pt-Mnz** and **Pt-COOH** prodrugs, were registered. A decrease in the height of the L3 edge peak indicates an intracellular Pt(IV) prodrug reduction. Using the a/b value, we estimated the percent of Pt(IV) in drug-preincubated tumor cells (Table 3). **Pt-COOH** demonstrated rapid release of cisplatin in the intracellular medium, with ∼80% of the **Pt-COOH** reduced in 2 h of incubation. Rapid intracellular biodegradation is common for Pt(IV) prodrugs, as was previously described for tetraplatin and satraplatin.[13,14]

Table 2. Coordination and a/b Ratio of XANES Spectra for Pt-COOH, Pt-Mnz, Cisplatin, and Oxoplatin

compound	coordination	a/b
cisplatin	$Pt^{II}Cl_2N_2$	1.45
oxoplatin	$Pt^{IV}Cl_2N_2O_2$	2.43
Pt-Mnz	$Pt^{IV}Cl_2N_2O_2$	2.24
Pt-COOH	$Pt^{IV}Cl_2N_2O_2$	2.67

In contrast, **Pt-Mnz** demonstrated unexpectedly high prodrug intracellular stability with only a 60% of **Pt-Mnz** reduced after 26 h of incubation. Uncommonly, **Pt-Mnz** accumulates in the cell as a Pt(IV) prodrug, which is followed by the gradual release of cisplatin; thus, the Pt(IV) prodrugs avoid rapid biodegradation.

Similar Pt(IV) prodrug metabolism studies using dried tumor cell samples were carried out (in addition to Hall's scientific group[64,65]) by Chen's[15,67,68] and Alina Nemirovski's[69,70] scientific groups. These works are devoted to the problems of rapid intracellular degradation of Pt(IV) prodrugs, as well as the study of the mechanism of Pt(IV) prodrug reduction. Previously reported XANES studies of the Pt(IV) intracellular metabolism demonstrated the rapid degradation of Pt(IV) samples in an intracellular medium. Only in the case of transplatin derivatives, Chen et al. demonstrated the intracellular stability of Pt(IV) prodrugs.[67] We had also reported an intracellular metabolism of the cisplatin-based **DNP** prodrug, which showed relative stability in tumor cells.[71] However, **Pt-Mnz** is reduced in the intracellular environment almost three times slower compared to **DNP**, thus being the most stable prodrug of the previously studied XANES method. The obtained results confirm the significant impact of the axial ligands on the intracellular reduction rate.[72−74]

Principles of Electrochemical Detection of Pt^{2+} Species via PtNE. The efficiency of clinical cancer therapy depends significantly on antitumor drugs being able to reach the therapeutic target. Electrochemical detection of Pt^{2+} species in biological objects based on a platinized nanoelectrode allows one to quantify the amount of platinum-based drugs directly inside a therapeutic target and thus evaluate the drug efficacy. Having previously succeeded in the electrochemical detection of cisplatin in cells, spheroids, and in vivo,[52,53] in this work, we evaluate a hypoxia-induced metabolism of the **Pt-Mnz** prodrug using the same approach. The three-dimensional (3D) spheroid proved to be a useful tool for studying hypoxia and hypoxia-activated agents given those cellular cultures are relatively close models of real tumors.[75−77]

To detect Pt^{2+} species at various depths of tumor spheroids, including hypoxia-associated areas, we utilized a 60 nm platinized carbon nanoelectrode (PtNE), a unique tool for the detection of different reactive species or drug metabolites in living systems. At different depths of the cellular spheroid, we recorded cyclic voltammograms from 400 to 1200 mV. The desired peak of Pt(II)/Pt(IV) oxidation is at 0.6−0.7 V vs Ag/AgCl, according to previously reported data[52,53] and preliminary experiments in cisplatin solutions. The calibration curve obtained from cyclic voltammetry (CV) in various cisplatin solutions allows us to quantify the Pt^{2+} level inside the spheroid and thus compare the Pt^{2+} accumulation level in spheroids, incubated with different Pt(IV) prodrugs or cisplatin. A principal scheme of an electrochemical experiment to detect Pt^{2+} species in biological objects is presented in Figure 3 and also in Figure S38, Supporting Information.

Metronidazole is selective for anaerobic bacteria as it is intracellularly reduced to nitroso-containing intermediates.[78,79] Metronidazole conjugated with cisplatin is expected to reduce deep in spheroids, thereby causing cisplatin to get stuck in the area of hypoxia. Using a unique PtNE tool for electrochemical measurements in single spheroids, we can also register the reduction of metronidazole inside spheroids.

PtNEs were prepared following a previously described procedure (Figure S39, Supporting Information).

Hypoxia Detection in a 3D Spheroid Tumor Model Using PtNE. We utilized the MCF-7 spheroid as the hypoxic tumor model. To confirm the presence of hypoxia inside MCF-

Table 3. Summary of the Extrapolated Percentage of Unreduced Pt(IV) for A549 Cells Incubated with Pt-Mnz or Pt-COOH

	Pt-Mnz		Pt-COOH	
incubation time (h)	a/b	% Pt^{IV}[a]	a/b	% Pt^{IV}[a]
0 (solid)	2.24 ± 0	100 ± 0	2.67 ± 0	100 ± 0
2	1.94 ± 0.03	61.34 ± 1.10	1.69 ± 0.02	21 ± 0.3
26	1.76 ± 0.06	41.66 ± 1.57	1.50 ± 0.02	6 ± 0.09

[a]Calculated using the corresponding derived linear function (Figure 2D).

https://doi.org/10.1021/acs.inorgchem.2c02062
Inorg. Chem. 2022, 61, 14705−14717

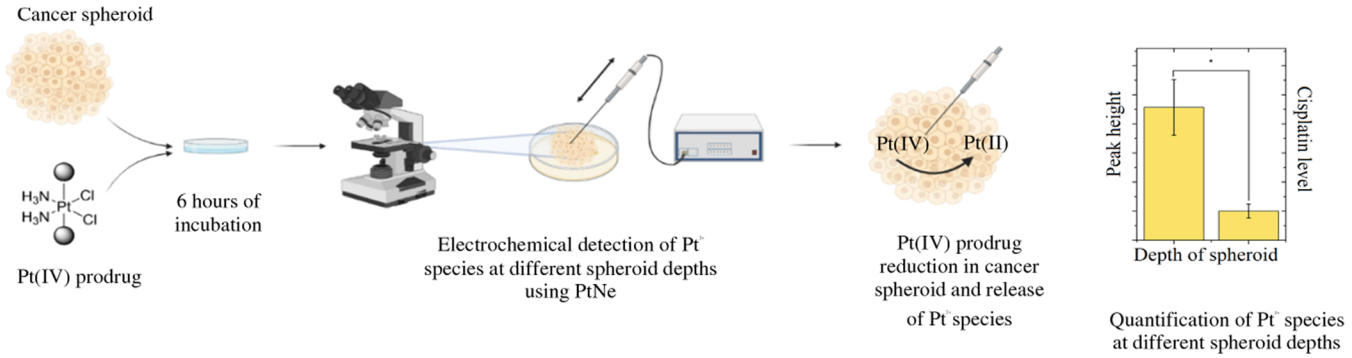

Figure 3. Principal scheme of the electrochemical experiment to detect Pt^{2+} species in cancer spheroids via PtNe. Spheroids were incubated with the Pt(IV) prodrug for 6 h; then, spheroids were transferred to the microscope in a fresh medium. PtNe was then inserted into the cancer spheroid, and cyclic voltammograms were recorded at different depths of the spheroid. Exemplary graph illustrating the Pt^{2+} species level at various depths of the spheroid. This image was created using biorender.com.

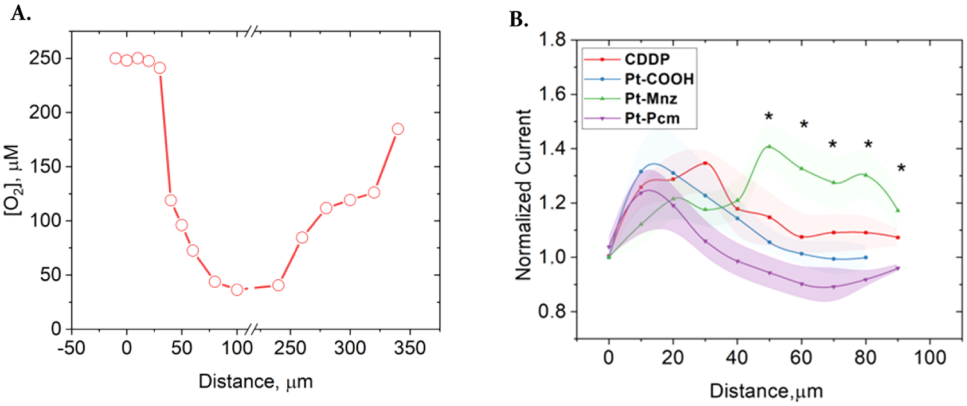

Figure 4. (A) Oxygen profile at various depths of MCF-7 spheroids measured by PtNE. (B) Biodistribution profile of Pt^{2+} species in MCF-7 spheroids preincubated with Pt(IV) prodrugs and cisplatin for 6 h. Normalized current depending on the distance from the MCF-7 spheroid surface, preincubated with **Pt-Mnz** (n = 3 spheroids), **Pt-COOH** (n = 4), **Pt-Pcm** (n = 4), and cisplatin (n = 3). The current is directly proportional to the Pt^{2+} concentration. The standard error is indicated by a colored background. *p < 0.05 (ANOVA).

7 spheroids, the oxygen profile at various depths in a spheroid was measured using an intracellular Pt-nanosensor. The O_2 level was calibrated using 2-point calibration (Figure S40, Supporting Information).[80] The pO_2 level inside the 3D tumor model was determined by the penetration of PtNE at various depths inside the spheroid (0−50 μm from the surface) (Figure S41, Supporting Information). The oxygen level was determined by current quantification at potential in the range of −500 to −600 mV ($O_2 + 4e^- + 4H^+ \rightarrow 2H_2O$).[80] At a depth of 40 μm, the oxygen level is decreased fivefold compared to the surface level (Figure 4A).

Detection of Pt^{2+} Species Inside MCF-7 Spheroids Using PtNE. To assess the ability of Pt(IV) prodrugs to accumulate in a hypoxic area deep in the spheroids, MCF-7 spheroids were incubated for 6 h with 100 μM Pt(IV) prodrugs. This incubation time was necessary for the prodrugs to be distributed throughout the volume of the spheroids and release the active Pt^{2+} species. MCF-7 spheroids preincubated with 100 μM cisplatin were used as positive controls. Preliminary measurements in a cisplatin solution and calibration of PtNE are presented in Figures S42 and S43, Supporting Information.

We then inserted the PtNE to various depths of spheroids to detect the signal of cisplatin (or its intracellular metabolites, Pt^{2+} species). Three/four spheroids were used in measurements for each Pt(IV) prodrug. On the resulting CV curves, a characteristic Pt(II)/Pt(IV) peak of oxidation was observed at approximately 800 mV. Compared to the peak of cisplatin oxidation obtained in the cisplatin solutions (~700 mV, Figure S42), a slight shift to the right is observed. This effect might be due to the intracellular metabolism of the drug, which was discussed previously.[52,53]

The combined results of CV measurements inside MCF-7 spheroids incubated with **Pt-Mnz**, **Pt-Pcm**, and **Pt-COOH** prodrugs and cisplatin show how the level of Pt^{2+} species varies as the depths of the spheroids increase (Figure 4B). The observed distribution profile of Pt^{2+} species is typical for spheroids: the highest Pt^{2+}concentration is near the spheroid surface; with the depth increasing, the Pt^{2+} species level decreases due to diffusion limitations.

For both prodrugs **Pt-COOH** and **Pt-Pcm**, the modes of Pt^{2+} biodistributions in spheroids are similar to those of cisplatin (Figure 4B, purple and blue tracks). **Pt-COOH**, despite its high lipophilicity (Table 1), does not accumulate in the hypoxic area of spheroids. A direct comparison of the ability to accumulate Pt^{2+} species in the spheroid of **Pt-COOH** and cisplatin clearly demonstrates that the rapid decay of Pt(IV) prodrugs equalizes their effectiveness. That is, the efficacy of the **Pt-COOH** and **Pt-Pcm** prodrugs does not differ from that of cisplatin, which is a common disadvantage of prodrugs.

https://doi.org/10.1021/acs.inorgchem.2c02062
Inorg. Chem. 2022, 61, 14705−14717

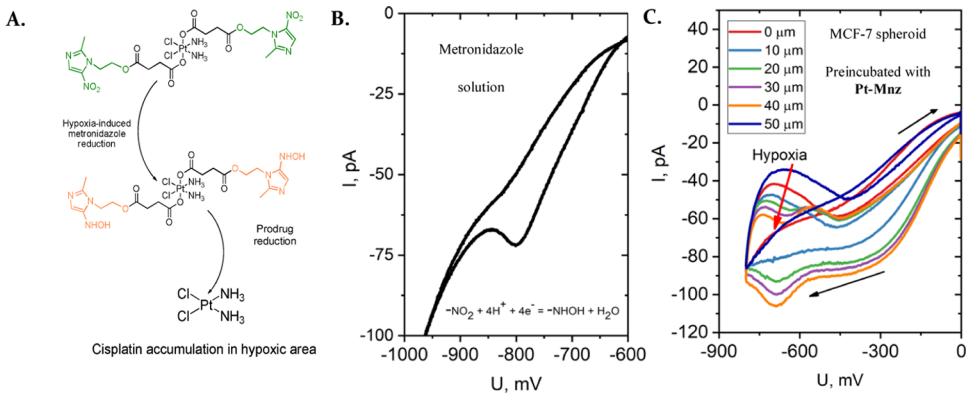

Figure 5. (A) Schematic representation of the **Pt-Mnz** intracellular metabolism. (B) Cyclic voltammograms of 1 mM metronidazole solution in PBS buffer measured by PtNE. The scan rate was 400 mV/s. (C) Voltammograms obtained at various depths of MCF-7 spheroids preincubated with **Pt-Mnz** for 2 h. Metronidazole reduction and oxygen depletion are highlighted by arrows. The scan rate was 400 mV/s.

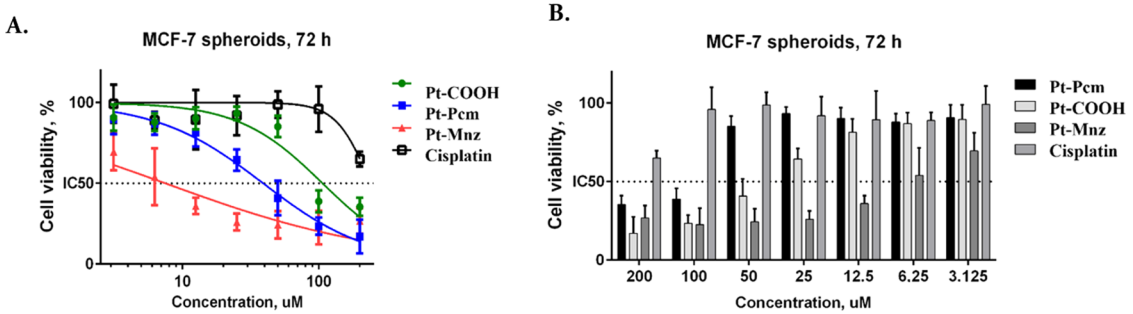

Figure 6. Cytotoxicity data for Pt(IV) prodrugs and cisplatin on MCF-7 spheroids after 72 h of incubation. (A) Cytotoxicity curves on MCF-7 spheroids for **Pt-COOH**, **Pt-Pcm**, **Pt-Mnz**, and cisplatin after 72 h of incubation. (B) Cell viability histogram of MCF-7 spheroids for **Pt-COOH**, **Pt-Pcm**, **Pt-Mnz**, and cisplatin.

The biodistribution profile of the **Pt-Mnz** prodrug is different from other drugs and cisplatin. In MCF-7 spheroids, preincubated with **Pt-Mnz** prodrug we detected Pt^{2+} species up to 100 micrometer depth of spheroids (Figure 4B, green track). **Pt-Mnz** shows an ability to accumulate Pt^{2+} species in the area of hypoxia, significantly surpassing the accumulation of **Pt-COOH**, **Pt-Pcm**, and cisplatin. Apparently, hypoxia-induced metronidazole reduction promotes the retention of **Pt-Mnz** in the spheroids, while the complex acts as a prodrug and gradually releases cisplatin. It is important that electrochemical detection could be realized within the whole volume of spheroids, while fluorescent labels[85] are usually specific for the outer layer (up to 50 μM) (Figure S48, Supporting Information).

Metronidazole Moiety Reduction in Living MCF-7 Spheroids. To confirm the role of the metronidazole moiety in the intraspheroidal behavior of **Pt-Mnz**, a reduction of the metronidazole moiety **Pt-Mnz** deep inside spheroids was assayed. Metronidazole reduction in hypoxic media has been repeatedly studied in vitro,[81−84] and intracellular reduction is presumed to occur by a similar mechanism. At first, an electrochemical study of a PBS buffer solution of metronidazole was performed via PtNE. Nitro-group reduction was determined in the −860 to −700 mV range ($-NO_2 + 4e^- + 4H^+ \rightarrow -NHOH + H_2O$).[57] The number of electrons was calculated according to the Laviron equation (Figures 5B and S49, Supporting Information).[86]

We then incubated the MCF-7 spheroid with **Pt-Mnz** for 2 h and electrochemically detected the reduction of metronidazole as the drug deepened into the area of hypoxia. A peak of about −700 mV, which corresponds to the reduction of metronidazole, gradually appears on intracellular voltammograms as the nanosensor depth increases in the spheroid preincubated with **Pt-Mnz** (Figure 5C). The lower the oxygen concentration in the spheroid, the higher the peak of the reduction of metronidazole to hydroxylamine Thus, hypoxia-sensitive metronidazole reduction was proved intravitally in an MCF-7 spheroid. This is the first confirmation of hypoxia-induced reduction detected electrochemically in single spheroids.

Cytotoxicity on 3D Spheroid Cellular Cultures. The obtained Pt^{2+} distribution profile for **Pt-Mnz** in MCF-7 spheroids allowed us to expect a high antiproliferative activity of **Pt-Mnz** in a 3D tumor model. Also, since the **Pt-Mnz** prodrug is supposed to act by retention of cisplatin in the area of hypoxia, the most indicative model to study its cytotoxicity is a 3D tumor model. Unlike monolayer cellular cultures, 3D spheroid cultures possess unique features that make them better hypoxic models of real tumors.[87] Thus, the antiproliferative activity of **Pt-Mnz** on spheroids is a clear marker that this Pt(IV) prodrug shows sensitivity to hypoxic conditions.

As can be seen from the obtained data, **Pt-Mnz** is more toxic than the reference Pt(IV) prodrugs or cisplatin (Figure 6), and the optical and confocal fluorescent images demonstrate the disruption of spheroids within incubation with **Pt-Mnz** (Figures S50 and S51 Supporting Information). Despite the fact that **Pt-Mnz** was not as effective on two-dimensional (2D) cell lines, in hypoxic spheroid models, it shows significant efficiency compared to cisplatin. The data obtained in the 3D tumor model revealed an increase in toxicity of **Pt-Mnz** by more than 31 times. This high efficacy of **Pt-Mnz** in 3D tumor

https://doi.org/10.1021/acs.inorgchem.2c02062
Inorg. Chem. 2022, 61, 14705−14717

models can be explained by the retention of the drug in the area of hypoxia.

CONCLUSIONS

We report herein the design, synthetic pathway, and thorough study of the biological activity of a novel Pt(IV) prodrug **Pt-Mnz** with metronidazole in the axial position. The nitroaromatic moiety in the **Pt-Mnz** complex was assumed to facilitate the delivery of the complex into oxygen-deficit hypoxia regions due to irreversible reduction of a nitro group. Two additional Pt(IV) prodrugs **Pt-COOH** and **Pt-Pcm** were designed as reference compounds with nonreducible axial ligands.

The intracellular reduction of **Pt-COOH** and **Pt-Mnz** was studied using the XANES technique. While **Pt-COOH** showed fast intracellular reduction, **Pt-Mnz** showed the ability to avoid rapid biodegradation. After 26 h of incubation in A549 tumor cells, only 60% of the **Pt-Mnz** was reduced, which indicates that **Pt-Mnz** does not reduce rapidly under biological conditions and instead slowly releases cisplatin in intracellular media.

An intravital electrochemical tracking of Pt^{2+} species release from different Pt(IV) prodrugs in a 3D cell culture was conducted using PtNE. After MCF-7 spheroids were incubated with equal doses of **Pt-Mnz**, **Pt-COOH**, **Pt-Pcm**, and cisplatin, Pt^{2+} species were registered through the whole depth of spheroids. Cisplatin, **Pt-COOH**, and **Pt-Pcm** showed a similar biodistribution profile, while **Pt-Mnz** showed the ability to deliver Pt^{2+} species to the area of deep hypoxia. Also, metronidazole moiety reduction as the **Pt-Mnz** deepens into a living MCF-7 spheroid was proved for the first time.

In support of the efficacy in hypoxic models, **Pt-Mnz** showed significant cytotoxicity on MCF-7 spheroids, 31-fold greater than that of cisplatin. We have demonstrated the key influence of the metronidazole moiety in the axial position on the accumulation of the **Pt-Mnz** prodrug in the area of deep hypoxia. Having synthesized structurally similar but more lipophilic drugs with nonreducible axial ligands and using them as reference compounds, we were convinced that lipophilicity is not a major factor in drug accumulation, compared to the hypoxia-sensitive reduction of the metronidazole axial ligand.

Thus, **Pt-Mnz** was proved to accumulate in the hypoxic area of 3D spheroids and release cisplatin under the influence of intracellular reductases in contrast to prodrugs without hypoxia-sensitive moieties. **Pt-Mnz** has greater potential compared with previously reported Pt(IV) analogues due to hypoxic-area accumulation, kinetic inertness, and slow release of cisplatin in tumor cells. The study shows that the combination of hypoxia-sensitive nitroaromatics and platinum complexes is a promising approach to treating oxygen-deficit solid tumors.

EXPERIMENTAL SECTION

Materials and Methods. Cisplatin, thiophosgene, glycine, glycine ethyl ester hydrochloride, 2-pyridinecarboxaldehyde, p-toluenesulfonyl chloride, benzyl alcohol, potassium hydroxide, 3-[bis(dimethylamino)methyliumyl]-3*H*-benzotriazol-1-oxide hexafluorophosphate (HBTU), dimethylaminopyridine (DMAP), and H_2O_2 37% w/w were purchased from commercial sources (Aldrich, Alfa, TCI, etc.) and used without further purification. Metronidazole and paracetamol were used in the form of pounded tablets; the admixtures were separated during the synthesis. Hydrochloric acid, N,N-dimethylformadide (DMF), toluene, MeOH, EtOH, and CH_2Cl_2 were purchased from Sigma Aldrich; dimethylsylfoxide (DMSO) was purchased from VMR (Life Science). Flash column chromatography (300−400-mesh silica gel) was performed for compound purification. Analytical thin-layer chromatography (TLC) was performed on Merck silica gel aluminum plates with the F-254 indicator. Compounds were visualized by irradiation with UV light or iodine staining. ^{1}H, ^{13}C, and ^{195}Pt NMR spectra were recorded on a Brucker-Avance instrument at 400 MHz (^{1}H), 101 MHz (^{13}C), and 86 MHz (^{195}Pt). Deuterochloroform ($CDCl_3$), deuteromethanol (CD_3OD), and dimethylsulfoxide-d6 (DMSO-d_6) were used as solvents. Chemical shifts are given in ppm on the δ scale relative to hexamethyldisiloxane as an internal standard. High-resolution mass spectra were recorded on an Orbitrap Elite mass spectrometer (Thermo Scientific). IR spectra were obtained on ThermoNicolet ISFT-IR. Liquid chromatography−mass spectrometry was performed by a Shimadzu Prominence LC-20 system with a column oven and a fraction collector coupled to a single quadrupole mass spectrometer Shimadzu LCMS-2020 with a dual DUIS-ESIAPCI ionization source. XANES spectra were measured at the L3 edge of platinum at the STM station of the Kurchatov Center of Synchrotron Radiation. The storage ring of the synchrotron is powered by an energy of 2.5 GeV; the average current in the ring is about 80 mA. The P content was determined by inductively coupled plasma mass spectrometry using an ICP-MS 7500a instrument (Agilent Technologies). The device was set up to work with solutions that have a low total concentration of solutes (RF power 1500 Vt, carrier gas flow rate 1.10 L/min, sample flow rate 0.4 mL/min, sampling depth 4 mm, t °C, 2 °C). Transfer and recording of measurements from PtNE to a computer were done using the ADC−DAC converter USB-6211 (National Instruments) and the program WinWCP (John Dempster, University of Strathclyde, U.K.). A micromanipulator PatchStar (Scientifica, Great Britain) was used to feed the nanosensor. All manipulations were made on the table of an optical inverted microscope (Nikon, Japan).

Synthesis and Characterization. *Oxoplatin (1).* Oxoplatin was synthesized according to the procedure published previously.[52] To 500 mg (1.67 mmol) of cisplatin, 30 mL of 30% hydrogen peroxide solution was added dropwise. The mixture was stirred at 75 °C for 5 h. The solution was left overnight at rt to form a yellowish precipitate. The precipitate formed was separated, the solvent was removed under reduced pressure, and the residue was collected with a small amount of water and washed subsequently with water, methanol, and diethyl ether and then air-dried. Yield: 515 mg, 92%. IR: 3459 (OH), 3149, 1583 (c), 1440 (c), 1378 (s), 1074 (s, Pt-OH), 860 (s), 574 (br. s).

(4-(2-(2-Methyl-5-nitro-1H-imidazol-1-yl)-4-oxobutanoic Acid)) 2. A total of 300 mg (1.75 mmol) of metronidazole was dissolved in 15 mL of acetonitrile; 264 mg (1.75 mmol) of succinic anhydride and 10 mg (5 mol %) of 4-dimethylaminopyridine (DMAP) were added. The resulting solution was stirred for 72 h at r.t., and the solvent was removed under reduced pressure. The resulting white precipitate was dissolved in methanol and centrifuged, and the solution was then evaporated and dried on air, giving 4-(2-(2-methyl-5-nitro-1*H*-imidazol-1-yl)-4-oxobutanoic acid) as a white powder. Yield: 354 mg (75%). ^{1}H NMR (400 MHz, CD_3OD, δ, ppm): 7.92 (s, 1H, C═CH−N), 4.65−4.63 (t, 2H, J = 4.93, $-CH_2-OH$), 4.45−4.42 (t, 2H, J = 4.93, CH_2-N), 2.51−2.49 (m, 7H, CH_3, CH_2-CH_2-COOH). ^{13}C NMR (101 MHz, DMSO-d_6, δ, ppm): 173.91 173.76, 173.29, 151.60, 133.40, 62.41, 44.76, 28.94, 28.51, 13.94. HRMS calculated $C_{10}H_{13}N_3O_6$ 272.0883 $(2 + H)^+$. Found $C_{10}H_{13}N_3O_6$ 272.0874 $(2 + H)^+$.

Pt-Mnz (3). A total of 90 mg (0.332 mmol) of (4-(2-(2-methyl-5-nitro-1*H*-imidazol-1-yl)-4-oxobutanoic acid)) **2** was dissolved in DMF; 0.05 mL (0.332 mmol) of triethylamine and 133 mg (0.332 mmol) of hexafluorophosphate (2-(1*H* benzotriazol-1-yl)-1,1,3,3-tetramethyluronium) (HBTU) were added. The mixture was stirred for 40 min at r.t. Then, 39 mg (0.117 mmol) of oxoplatin **1** was added, and the resulting solution was stirred for 48 h at r.t. The solvent was removed under reduced pressure, 3 mL of methanol was added to the residue, and the solution was precipitated with an excess of diethyl ether. The solution was centrifuged, and the residue was air-dried, washed with ether, centrifuged, and air-dried again, giving Pt-Mnz as a beige powder. 52 mg, 53%. ^{1}H NMR spectrum (400 MHz,

https://doi.org/10.1021/acs.inorgchem.2c02062
Inorg. Chem. 2022, 61, 14705−14717

DMSO-d_6, δ, ppm): 8.04 (s, 2H, C═CH−N), 6.48 (br.s., 6H, NH_3), 4.58−4.55 (t, 4H, J = 4.93, $-CH_2-OH$), 4.38−4.36 (t, 4H, J = 4.93 Hz, CH_2-N), 2.46 (s, 6H, CH_3), 2.46−2.44 (m. 4H, CH_2-COO-Mnz), 2.39−2.35 (t, 4H, J = 5.87 Hz, $-CH_2-COOPt$). ^{13}C NMR (101 MHz, DMSO-d_6, δ, ppm): 207.34, 179.38, 172.32, 152.05, 133.51, 62.60, 45.20, 31.13, 29.90, 14.46. ^{195}Pt NMR (86.07 MHz, DMSO-d_6, δ, ppm): 1226.46. HRMS calculated $C_{20}H_{29}Cl_2N_8O_{12}Pt^-$ 838.0930 $(3-H)^-$. Found $C_{20}H_{29}Cl_2N_8O_{12}Pt^-$ 838.0395 $(3-H)^-$.

Isothiocyanatoethyl Acetate ***4***. In a three-necked flask, 27 g (0.192 mol) of glycine ethyl ester hydrochloride was dissolved in a mixture of CH_2Cl_2/H_2O (80/80 mL). Using two dropping funnels, 50.4 g (0.6 mol) of $NaHCO_3$ in 200 mL of H_2O and 23 g (0.2 mol) of $CSCl_2$ in 80 mL of CH_2Cl_2 solutions were added simultaneously with stirring. The mixture was stirred for 3 h. Upon completion of the reaction, the organic solution had a light-yellow color, and the aqueous layer was colorless. The organic layer was separated on a separatory funnel and washed with water and brine (3 × 30 mL). The combined organic fractions were dried over anhydrous sodium sulfate. The solvent was removed under reduced pressure. The resulting dark-orange oil was distilled under a vacuum (T = 76 °C/5 mmHg); isothiocyanatoethyl acetate **4** was obtained as a light-yellow oil. Yield: 24 g, 86%. ^1H NMR (400 MHz, $CDCl_3$. δ, ppm): 4.30−4.26 (q, J = 7.09 Hz, 2H, $-CH_2^-$), 4.23 (s, 2H, CH_2NCS), 1.33−1.30 (t, 3H, J = 7.09 Hz, CH_3). ^{13}C NMR (101 MHz, DMSO-d_6, δ, ppm): 165.76, 62.24, 46.02, 13.72.

((Z)-2-(5-Oxo-4-(pyridine-2-ylmethylene)-2-thioxoimidazolidin-1-yl) Acetate) ***5***. A total of 735 μL (5.9 mmol) of isothiocyanate ethyl acetate **4** and 830 μL (5.9 mmol) of triethylamine were added dropwise to a solution of 2 g (5.9 mmol) of glycine benzyl ester p-toluenesulfonic salt in 10 mL of methanol. The mixture was stirred overnight at r.t.; then, the solvent was removed under reduced pressure. To the precipitate formed, 30 mL of EtOH and 365 mg (6.5 mmol) of potassium hydroxide were added and 625 μL (6.5 mmol) of 2-pyridinecarbaldehyde was added dropwise to form a red mixture, which was stirred for 2 h at r.t. The solution was acidified to pH = 7 with 0.1 M hydrochloric acid; the yellow precipitate formed was filtered, washed with EtOH, and dried on air. The product was purified by column chromatography (CH_2Cl_2/MeOH 20:1). Then, 853 mg (37%) of ethyl (Z)-2-(5-oxo-4-(pyr-idin-2-ylmethylene)-2-thioxoimidazolidin-1-yl) acetate **5** was obtained as a yellow powder. Yield: 853 mg (37%). ^1H NMR (400 MHz, DMSO-d_6, δ, ppm): 11.93 (s, 1H, NH), 8.73−8.71 (d, 1H, J = 4.89 Hz, Hα''-Py), 7.89−7.86 (t, 1H, J = 7.83 Hz, Hγ-Py), 7.74−7.72 (d, 1H, J = 7.82 Hz, Hβ-Py), 7.39−7.36 (m, 1H, Hβ''-Py), 6.80 (s, 1H, CH═), 4.60 (s, 2H, $CH_2-COOEt$), 4.17−4.11 (td, 2H, J = 7.83 Hz, CH_2-CH_3), 1.20−1.16 (t, 3H, J = 7.83 Hz, CH_2-CH_3). ^{13}C NMR (101 MHz, DMSO-d_6, δ, ppm): 177.31, 166.83, 163.05, 152.72, 149.88, 137.49, 129.19, 126.89, 123.53, 109.80, 61.50, 41.71, 14.01. HRMS calculated 292.0756 $(5+H)^+$. Found $C_{13}H_{14}N_3O_3S^+$ 292.0754 $(5+H)^+$.

(Z)-3-(5-Oxo-4-(pyridine-2-ylmethylene)-2-thioxoimidazolidin-1-yl) Acetic Acid ***6***. A total of 853 mg (2.9 mmol) of (Z)-2-(5-oxo-4-(pyridine-2-ylmethylene)-2-thioxoimidazolidin-1-yl) acetate **5** was dissolved in 120 mL of water; then, 197 mg (3.5 mmol) of potassium hydroxide was added. The solution was stirred for 3 h at r.t. Then, 1 N hydrochloric acid was added dropwise (until pH = 7), and a light-yellow precipitate was obtained as a result. The reaction mixture was extracted with diethyl ether (3 × 100 mL); the organic fractions were combined and dried over sodium sulfate, and the solvent was evaporated under reduced pressure. The product was purified by column chromatography (CH_2Cl_2/MeOH/AcOH 20:1:1%). (Z)-3-(5-Oxo-4-(pyridin-2-ylmethylene)-2-thioxoimidazolidin-1-yl) acetic acid **6** was obtained as a yellow powder. Yield: 512 mg, 66%. ^1H NMR (400 MHz, DMSO-d_6, δ, ppm): 13.26 (br, 1H, OH), 11.93 (br, 1H, NH), 8.75−8.73 (d, 1H, J = 4.89 Hz, Hα'-Py), 7.91−7.88 (td, 1H, J_1 = 7.83 Hz, J_2 = 1.96 Hz, Hγ-Py), 7.76−7.74 (d, 1H, J = 7.83 Hz, Hβ-Py), 7.41−7.36 (m, 1H, Hβ'-Py), 6.82 (s, 1H, CH═), 4.51 (s, 2H, CH_2-COOH). ^{13}C NMR (101 MHz, DMSO-d_6, δ, ppm): 177.54, 168.15, 163.15, 152.84, 149.92, 137.49, 129.30, 126.87, 123.50, 109.58, 41.78. HRMS calculated $C_{11}H_8N_3O_3S^-$ 262.0286 $(6-H)^-$. Found $C_{11}H_8N_3O_3S^-$ 262.0293 $(6-H)^-$.

*Pt-COOH (****7****).* A total of 98 mg (0.37 mmol) of (Z)-3-(5-oxo-4-(pyridin-2-ylmethylene)-2-thioxoimidazolidin-1-yl) acetic acid **6** was dissolved in 5 mL of DMF; 52 μL (0.37 mmol) of triethylamine and 142 mg (0.37 mmol) of hexafluorophosphate 2-(1*H* benzotriazol-1-yl)-1,1,3,3-tetramethyluronium (HBTU) were added. The solution was stirred for 40 min at r.t. Then, 50 mg (0.15 mmol) of oxoplatin **1** was added, and the resulting solution was stirred at r.t. for 48 h. The solvent was removed under reduced pressure, and the product was purified by column chromatography (CH_2Cl_2:MeOH 20:1), giving Pt-COOH as an orange powder. Yield: 30 mg, 25%. ^1H NMR (400 MHz, DMSO-d_6, δ, ppm): 11.78 (br.s., 2H, NH), 8.73−8.72 (d, 2H, J = 3.91 Hz, Hα'-Py), 7.89−7.85 (td, 2H, J_1 = 7.83 Hz, J_2 = 1.96 Hz, Hγ-Py), 7.73−7.71 (d, 2H, J = 7.83 Hz, Hβ-Py), 7.38−7.35 (m, 2H, Hβ'-Py), 6.74 (s, 2H, CH═), 6.48 (br.s., 6H, NH_3), 4.57 (s, 4H, CH_2-COOPt). ^{13}C NMR (101 MHz, DMSO-d_6, δ, ppm): 178.00, 174.06, 163.51, 153.34, 150.32, 137.90, 129.81, 127.19, 123.81, 109.40, 40.86. ^{195}Pt NMR (86 MHz, DMSO-d_6 δ, ppm): 1250.92. HRMS calculated $C_{22}H_{23}Cl_2N_8O_6PtS_2^{-822.0050}$ $(7-H)^-$. Found $C_{22}H_{23}Cl_2N_8O_6PtS_2^+$ 822.0058 $(7-H)^-$.

(4-(4-Acetamidophenoxy)-4-oxobutanoic Acid) ***8***. A total of 662 mg (6.6 mmol) of succinic anhydride was suspended in 2.5 mL of toluene and cooled to 0 °C. Under an inert atmosphere, 1 g (6.6 mmol) of paracetamol and 265 mg (6.6 mmol) of NaOH in 2.5 mL of water were added over 15 min. Then, the solution was stirred for 1.5 h in an ice bath under an inert atmosphere. The mixture was centrifugated, and the aqueous layer was acidified with 1 N HCl until the formation of a whiteish precipitate, which was dissolved in the saturated solution of $NaHCO_3$ and then acidified with 1 N HCl until pH = 3. The product was purified by column chromatography CH_2Cl_2/MeOH/AcOH (20:1:1%), giving 4-(4-acetamidophenoxy)-4-oxobutanoic acid as a white powder. Yield: 354 mg, 22%. ^1H NMR (400 MHz, DMSO-d_6, δ, ppm): 10.09 (s, 1H, NH), 7.58−7.56 (d, 2H, J = 8.53 Hz, H-Ph), 6.98−6.95 (d, 2H, J = 8.53 Hz, H-Ph), 2.74−2.71 (t, 2H, J = 6.09 Hz, CH_2-COOR), 2.56−2.53 (t, 2H, J = 6.09 Hz, CH_2-COOH), 2.01 (s, 3H, CH_3).

*Pt-Pcm (****9****).* A total of 67 mg (0.267 mmol) of 4-(4-acetamidophenoxy)-4-oxobutanoic acid **8** was dissolved in DMF; 0.038 mL (0.267 mmol) of triethylamine and 102 mg (0.267 mmol) of hexafluorophosphate (2-(1*H*-benzotriazol-1-yl)-1,1,3,3-tetramethyluronium) (HBTU) were added, and the mixture was stirred for 40 min at r.t. Then, 30 mg (0.09 mmol) of oxoplatin **1** was added, and the resulting solution was stirred for 48 h at r.t. The solvent was removed under reduced pressure; 2 mL of methanol was added to the residue, and the product was precipitated with diethyl ether. The whiteish precipitate formed was centrifuged, and the residue was dried on air, giving Pt-Pcm as a beige powder. Yield: 24 mg, 33%. ^1H NMR (400 MHz, DMSO-d_6, δ, ppm): 10.23 (s, 2H, NH), 7.62−7.60 (d, 4H, J = 9.14 Hz, Ph-H), 7.06−7.04 (d, 4H, J = 8.53 Hz, Ph-H), 6.61 (br s, 6H, NH_3), 2.70−2.64 (m, 8H, CH_2-CH_2-COOR), 2.04 (s, 6H, CH_3). ^{13}C NMR (101 MHz, DMSO-d_6, δ, ppm): 179.60, 171.72, 168.61, 146.17, 137.28, 122.35, 120.17, 30.84, 30.33, 9.08. HRMS calculated $C_{24}H_{30}Cl_2N_4O_{10}Pt^+$ 800.10596 $(9+H)^+$. Found $C_{24}H_{30}Cl_2N_4O_{10}Pt^+$ 800.1079 $(9+H)^+$.

HPLC Analysis. HPLC was carried out on an Acclaim RSLC 120 C18 column (Dionex, United States), 3.0 mm × 75 mm, particle size 3 μm, in the isocratic mode. The mobile phase was a mixture of deionized water with methanol containing 0.1% formic acid. The eluent feed rate was 0.5 mL/min, and the column thermostat temperature was 40 °C. Detection was carried out in the wavelength range of 250−600 nm. For Pt-Mnz, 30% of the MeOH in the mobile phase was used; for Pt-Pcm and Pt-COOH, 35 and 50% were used, respectively.

Stability Study of Pt^{IV} Prodrugs in Neutral Conditions. A 1 mM solution of **Pt-Mnz**, **Pt-COOH**, or **Pt-Pcm** in the presence of 0.1 M ammonium acetate in 1.2 mL of a H_2O/acetonitrile/DMSO mixture (1:1:0.1) was kept at 37°C, and 20 μL samples were taken at 5 min, 15 min, 30 min, 1 h, 2 h, 4 h, 6 h, and 24 h, which were then analyzed by HPLC.

Cyclic Voltammetry and Differential Pulse Voltammetry Assay. Electrochemical measurements were performed with a

https://doi.org/10.1021/acs.inorgchem.2c02062
Inorg. Chem. 2022, 61, 14705−14717

potentiostat/galvanostat PamlSens 3 (PalmSens, Netherlands). Cyclic voltammetry (CV) and differential pulse voltammetry (DPV) were carried out in a three-compartment electrochemical cell containing a glassy carbon working electrode and an auxiliary electrode and Ag|AgCl in a 1 M KCl reference electrode. The surfaces of glassy carbon electrodes (r = 1 mm) in Teflon bodies were polished before each measurement using Al_2O_3 (10 and 0.05 μm) and a wet microcloth pad in distilled water. Between the individual polishing steps, the electrodes were rinsed with distilled water. The electrochemical cell was filled with a supporting electrolyte: phosphate-buffered saline (50 mM) with pH 7.4, containing 180 mM NaCl and 5% DMSO in distilled water. The working electrode compartment was filled with metronidazole or its complex with Pt (~1 mM) dissolved in the supporting electrolyte.

Cell Lines and Culture Conditions. Human embryonic kidney HEK-293T, human breast adenocarcinoma MCF-7 and 4T1, human lung carcinoma A-549, and lung fibroblast Va13 cells were used. All cells were cultured in a DMEM/F12 (Gibco) culture medium supplemented with 10% fetal bovine serum (Gibco), 50 U/mL penicillin, 0.05 mg/mL streptomycin (Gibco), and 1 × Glutamax (Gibco). Cell cultures were tested for the absence of mycoplasma.

Inhibition of the Cell Viability Assay. The cytotoxicity assay was performed using the automatic station Janus (Perkin). For this, a cell suspension (2500 cells for HEK-293T, MCF-7, and A-549; 4000 cells for Va13) in 140 μL of DMEM/F12 media was added in 96-well plates. Cells were incubated at 37 °C in a CO_2 incubator for 24 h. Stock DMSO solutions of drugs (10 mM) were prepared and then diluted with a full medium just prior to the experiment. The maximum drug concentration was 100 μM, while the DMSO concentration did not exceed 1% by volume. All experiments were performed in triplicate. After 72 h, the MTT reagent (3-(4,5-dimethylthiazol-2-yl)-2,5-diphenyltetrazolium bromide) (Paneco) was added to the cells to a final concentration of 0.5 g/L. Cells were incubated with the MTT reagent for 2 h at 37 °C in a CO_2 incubator. Next, the medium with the MTT reagent was decanted, and 140 μL of DMSO was added. Cells were incubated with DMSO for at least 15 min at rt using an orbital shaker to dissolve the formazan formed during the reduction of the MTT reagent. The optical absorption of formazan was measured at a wavelength of 565 nm using a VICTOR X5 plate reader. A nonlinear regression model, in which four parameters were evaluated (lower limit, upper limit, slope, ED_{50}), was found for each drug using drc and drexplorer software packages for RStudio.

Cellular Platinum Accumulation and Distribution. Human breast adenocarcinoma cells MCF-7 (4T1) were cultured in DMEM/F12 supplemented with 10% FBS and 1% glutamine. The stock DMSO solutions of drugs (10 mM) were prepared and then diluted with a full medium prior to the experiment. The cells were incubated with 4 mL of prepared solutions in a CO_2 incubator at 37 °C. After 24 h, the medium was decanted, and the cells were washed twice with PBS (10 mM, 7.4) and collected by trypsinization. The cell suspension was centrifuged at 2500 rpm for 5 min in a Beckman centrifuge. The collected cells were resuspended in 1 mL of PBS and counted using a TC20 automated cell counter (Biorad). Cell samples are divided into fractions by the differential centrifugation method. Platinum concentration was determined by ICP-MS. The detection limit did not exceed 0.00001 mg/L. The relative error of determination did not exceed 3%. Pt determination was performed according to m/z 195. The instrument was calibrated using multielement standard solutions. The concentration range of the determined elements in standard solutions was 0.001−1.0 mg/L. To ensure the stability of the instrument and increase the reproducibility of the results, the analysis was performed with an automatic addition of an internal standard containing Li, Sc, Ge, Y, In, Tb, and Bi to the analyzed samples.

XANES Spectra of Solid Samples. The XANES spectra were measured at the L3 edge of platinum. All spectra were measured in the fluorescence signal detection mode using an Amptek FASTSDD detector. The spectrum of the Amptek detector was normalized using the current of the ionization chamber, which was used as a detector of X-rays incident on the sample. For monochromatization of the beam, a slotted monochromator based on a silicon single crystal with a reflecting surface was used with the standard energy resolution reaching $\Delta E/E \sim 2 \times 10^{-4}$. Energy calibration was performed by measuring the spectrum of the platinum foil and calibrating the monochromator to the maximum of the spectrum. To obtain a satisfactory signal-to-noise ratio for each sample, 16 spectra were measured for cell samples, and each spectrum took about 30 min. For solid Pt^{II} and Pt^{IV} complexes, three spectra were measured for each sample. In the Athena (Iffefit) program, the spectra were averaged and normalized. The measurement error is estimated as the ratio of the square root of the total accumulated signal to the total useful signal. For experimental data, the error is no more than 5% of the normalized absorption spectrum. For solid Pt^{II} and Pt^{IV} samples, the measurement error was negligible.

XANES Spectra of Dried Drug-Preincubated A549 Cell Samples. Human lung carcinoma A549 cells were seeded in T25 culture flasks (700 000 cells per flask). After incubation for 40 h and reaching 80% confluence, 10 mM DMSO solutions of **Pt-Mnz** and **Pt-COOH** were added for 2 or 26 h. Following the incubation, the drug-containing medium was removed, and the cells were washed thoroughly with ice-cold PBS solution (pH 7.5, SIGMA) to remove the residual medium. The cells were trypsinized and centrifuged at 2500 rpm for 3 min, the supernatant was removed, and the cells were resuspended in a solution of ammonium acetate (100 mM, 5 mL) and centrifuged again. Finally, the cell pellets were washed with a 70% ethanol solution, yielding a dry cell pellet. The samples were immediately freeze-dried for 24 h and stored in a desiccator until they were analyzed. At the time of analysis, the freeze-dried cells were packed into a polycarbonate sample holder, and the open face was secured with a Kapton tape (Kapton) window for XANES analysis. The XANES spectra of the L3 edge of platinum were recorded in the fluorescence signal detection mode.

PtNE Preparation. For PtNE preparation, commercially available disk-shaped carbon nanoelectrodes isolated in quartz (ICAPPIC Limited, U.K.) with diameters of 60−100 nm were used. To increase the adhesion of platinum to the surface of the carbon nanoelectrode, we created a nanoscale cavity according to the previously described technique.[50] Etching was performed in a 0.1 M NaOH solution with 10 mM KCl applying a symmetric V-shaped protocol with an amplitude of 1.5−2 V vs Ag/AgCl. Electrochemical deposition of platinum was achieved by potential cycling from 0 to −0.8 V with a scan rate of 200 mV/s in a 2 mM H_2PtCl_6 solution in 0.1 hydrochloric acid. The potential difference between the PtNE and the reference electrode was recorded by a patch-clamp amplifier Model 2400 (A-M Systems).

Calibration of PtNE with Cisplatin Solutions. To calibrate PtNE with cisplatin, 1000, 500, 10, and 1 μM solutions of cisplatin were prepared in HBSS buffer. Cyclic voltammetry from 0 to 1400 mV vs Ag/AgCl with a scan rate of 330 mV/s was recorded. The calibration curve was plotted at 1000 mV.

O_2-Level Determination in MCF-7 Spheroids by PtNE. The pO_2 level was determined using PtNE at various depths inside the MCF-7 spheroid (0−50 μm above the surface) in the range from −500 to −600 mV ($O_2 + 4e^- + 4H^+ \rightarrow 2H_2O$).

Pt^{2+} Species Detection in MCF-7 Spheroids Preincubated with Pt(IV) Prodrugs by PtNE. The spheroids were placed in 96-well plates coated with agarose. Spheroids from the plate were seeded onto 35 mm TC-treated Petri dishes (Eppendorf) 1 day before the experiment. Next, 1.55 mL of Dulbecco's modified Eagle's medium (DMEM)/F12 medium supplemented with 10% FBS was added to each Petri dish. Spheroids were incubated overnight in a CO_2 incubator at 37 °C to attach to the bottom of the Petri dish. The next day, an aliquot of Pt(IV) prodrugs or cisplatin was added to the spheroids to the total concentration of each compound (100 μM). Spheroids were then incubated for 6 h at 37 °C in a CO_2 incubator. Before the electrochemical measurements, the cell culture medium was replaced with Hanks' balanced salt solution (HBSS) buffer. Cisplatin accumulation was measured in the range corresponding to Pt(II) oxidation. Untreated spheroids were used as controls. PtNE

https://doi.org/10.1021/acs.inorgchem.2c02062
Inorg. Chem. 2022, 61, 14705−14717

was brought to the spheroid using a manipulator. A potential from 0 to 1400 mV vs Ag/AgCl (sweep speed 330 mV/s) was used. The Pt oxidation signal in spheroids was determined at various depths by the penetration of the spheroid by PtNE and recording the CV at various depths inside the spheroids (0−200 μm above the surface) in the range of 900−1200 mV vs Ag/AgCl.

Metronidazole Reduction in Phosphate-Buffered Solution. A 4 mM metronidazole solution was prepared in 0.01 M phosphate buffer with 0.137 M NaCl. Electrochemical measurements were performed using nanoelectrodes (carbon and platinum). The peak was shifted when measured by various types of electrodes (Pt or carbon), but not so significantly (−860 mV for a Pt electrode and −805 mV for a carbon electrode). Nitro-group reduction was determined in the range from −860 to −700 mV ($NO_2 + 4e^- + 4H^+ \rightarrow NHOH + H_2O$). The number of electrons was calculated according to the Laviron equation.

Pt-Mnz Axial Ligand Reduction in MCF-7 Spheroids. MCF-7 spheroids were incubated with 45 μM **Pt-Mnz** at 37 °C for 2 h. For further electrochemical measurements, the cell culture medium was replaced with HBSS buffer. Electrochemical measurements were performed using PtNEs. **Pt-Mnz** reduction was determined in the range from −860 to −700 mV ($NO_2 + 4e^- + 4H^+ \rightarrow NHOH + H_2O$).

Cytotoxicity in Tumor Spheroids (MTS Assay). Tumor spheroid formation was performed using the liquid overlay technique with agarose-coated plates, as has been described earlier.[88] Briefly, 1.5% wt of agarose in PBS (pH 7.4) was heated on a water bath for 15 min. Then, 50 μL of melted agarose was added to each well of a flat-bottom 96-well plate under sterile conditions. Plates with agarose were cooled down to r.t. for 15 min. Cells were seeded on agarose-coated plates (10 000 cells/well, 100 μL of media per well) and incubated at 37 °C and 5% CO_2 for 72 h to generate spheroids. The formation of tumor spheroids was observed using an inverted light microscope. Then, the solutions (1−200 μM) of CDDP and Pt(IV) prodrugs were added to spheroids for 72 h. The cytotoxicity was evaluated using a colorimetric MTS assay based on the NAD(P)H-dependent dehydrogenase activity, resulting in the reduction of the MTS tetrazolium compound and the generation of the soluble formazan product in cell culture media. The formazan formation was measured at 490 nm using a Varioskan Flash reader (Thermo Scientific). The IC_{50} values were estimated using GraphPad Prism Software (ver, 6.01) as the mean value of all experiments ± SD

Cytotoxicity in Tumor Spheroids (Calcein AM Staining). Tumor spheroids were incubated with Pt(IV) prodrugs (20 and 200 μM) for 48 h and stained with Calcein AM (50 μM, 30 min in a CO_2 incubator). The fluorescence of Calcein AM was measured with a Leica TCS SPE confocal system, excitation 488 nm, and emission 510−600 nm.

Pt^{2+} Species Detection in MCF-7 Spheroids Preincubated with Pt(IV) Prodrugs Using an FDCPt1 Fluorescence Probe. MCF-7 spheroids were obtained using agarose-coated plates, as described above. Then, the spheroids were treated with Pt-Mnz or cisplatin at 100 μM for 6 h at 37 °C in a 5% CO_2 incubator. After the incubation, spheroids were washed with PBS, followed by staining with FDCPt1[53,85] diluted in PBS (100 μM) for 30 min at 37 °C and 5% CO_2, according to the protocol of Shen et al. (68). Then, the spheroids were washed again with PBS and fixed with 4% formaldehyde solution in PBS for 15 min at r.t. Spheroids were imaged on a Leica TCS SPE confocal microscopy system using a 488 nm excitation laser and a 10× objective. Images were edited using LAS AF lite software (Leica, Germany).

■ ASSOCIATED CONTENT

Supporting Information

The Supporting Information is available free of charge at https://pubs.acs.org/doi/10.1021/acs.inorgchem.2c02062.

Synthetic schemes; $E_{1/2}$ potential values for Pt(IV) prodrugs; IC_{50} values of Pt(IV) prodrugs; intracellular accumulation and distribution of **Pt-Mnz** and **Pt-COOH** in MCF-7 cells; IR spectrum of **1**, ^1H NMR and ^{13}C NMR spectra of compounds **2**−**9**; ^{195}Pt NMR spectra of **Pt-Mnz** and **Pt-COOH**; HRMS spectra of **3, 6, 7**, and **9**; HPLC data for **Pt-Mnz** and **Pt-COOH**; stability of Pt(IV) prodrugs; CV of **Pt-Mnz** and **Pt-COOH**; SWV of **Pt-Mnz**; cytotoxicity curves for **Pt-Mnz**, **Pt-COOH**, and **Pt-Pcm**; cellular distribution graphs in MCF-7 cells for **Pt-Mnz** and **Pt-COOH**; PtNE scheme and preparation; PtNE calibration oxygen measurement in MCF-7 spheroids by PtNE; voltammogram of cisplatin; peak current dependence on cisplatin concentration; voltammograms at different depths of MCF-7 spheroids incubated with cisplatin; **Pt-Mnz, Pt-COOH**, and **Pt-Pcm** voltammograms of metronidazole measured by PtNE; cyclic voltammograms with metronidazole reduction peaks obtained at different depths of the MCF-7 spheroid; and preincubated with **Pt-Mnz** (PDF)

■ AUTHOR INFORMATION

Corresponding Author

Olga O. Krasnovskaya − *Chemistry Department, Lomonosov Moscow State University, Moscow 119991, Russia; National University of Science and Technology (MISIS), Moscow 119049, Russia;* orcid.org/0000-0002-4948-2747; Email: krasnovskayao@gmail.com

Authors

Daniil V. Spector − *Chemistry Department, Lomonosov Moscow State University, Moscow 119991, Russia; National University of Science and Technology (MISIS), Moscow 119049, Russia*

Alexander S. Erofeev − *Chemistry Department, Lomonosov Moscow State University, Moscow 119991, Russia; National University of Science and Technology (MISIS), Moscow 119049, Russia*

Petr V. Gorelkin − *National University of Science and Technology (MISIS), Moscow 119049, Russia*

Alexander N. Vaneev − *Chemistry Department, Lomonosov Moscow State University, Moscow 119991, Russia; National University of Science and Technology (MISIS), Moscow 119049, Russia;* orcid.org/0000-0001-8201-8498

Roman A. Akasov − *I.M. Sechenov First Moscow State Medical University, Moscow 119991, Russia; Federal Scientific Research Center "Crystallography and Photonics" Russian Academy of Sciences, Moscow 119333, Russia;* orcid.org/0000-0001-6486-8114

Nikolay V. Ul'yanovskiy − *Core Facility Center "Arktika," Northern (Arctic) Federal University, Arkhangelsk 163002, Russia*

Vita N. Nikitina − *Chemistry Department, Lomonosov Moscow State University, Moscow 119991, Russia*

Alevtina S. Semkina − *Pirogov Russian National Research Medical University (RNRMU), Moscow 117997, Russia; Department of Basic and Applied Neurobiology, Serbsky National Medical Research Center for Psychiatry and Narcology, Moscow 119034, Russia*

Kseniya Yu Vlasova − *Chemistry Department, Lomonosov Moscow State University, Moscow 119991, Russia; Pirogov Russian National Research Medical University (RNRMU), Moscow 117997, Russia;* orcid.org/0000-0003-3774-1323

https://doi.org/10.1021/acs.inorgchem.2c02062
Inorg. Chem. 2022, 61, 14705−14717

Mikhail A. Soldatov − *The Smart Materials Research Institute Southern Federal University Sladkova, Rostov-on-Don 344090, Russia;* orcid.org/0000-0003-1918-7875
Alexander L. Trigub − *National Research Center "Kurchatov Institute", Moscow 123182, Russia*
Dmitry A. Skvortsov − *Chemistry Department, Lomonosov Moscow State University, Moscow 119991, Russia*
Alexander V. Finko − *Chemistry Department, Lomonosov Moscow State University, Moscow 119991, Russia*
Nikolay V. Zyk − *Chemistry Department, Lomonosov Moscow State University, Moscow 119991, Russia*
Dmitry A. Sakharov − *Mendeleev University of Chemical Technology of Russia, Moscow 125047, Russia*
Alexander G. Majouga − *Chemistry Department, Lomonosov Moscow State University, Moscow 119991, Russia; National University of Science and Technology (MISIS), Moscow 119049, Russia; Mendeleev University of Chemical Technology of Russia, Moscow 125047, Russia;* orcid.org/0000-0002-5184-5551
Elena K. Beloglazkina − *Chemistry Department, Lomonosov Moscow State University, Moscow 119991, Russia;* orcid.org/0000-0001-6796-8241

Complete contact information is available at: https://pubs.acs.org/10.1021/acs.inorgchem.2c02062

Author Contributions

O.O.K. and D.V.S. designed the project and devised the experiments. All authors contributed to the discussions and manuscript preparation.

Funding

Electrochemical experiments with biological models were supported by the Russian Science Foundation (Grant No. 20-14-00312). Cytotoxicity tests were supported by the Russian Science Foundation (Grant No. 21-64-00006). All experiments with spheroids were supported by the Ministry of Science and Higher education within the State assignment FSRC "Crystallography and Photonics".

Notes

The authors declare no competing financial interest.

■ ACKNOWLEDGMENTS

The authors are grateful to the Kurchatov Institute for the beamtime, as well to the SMT station and Alexander Trigub for recording the XANES spectra of solid drug samples and dried tumor cells and processing the results. The authors are also grateful to Mikhail Soldatov for his help in preparing the XANES experiment and processing the results. The authors also thank Dmitrii Vinogradov (ITMO university, Saint-Peterburg, Russia) for images created with Biorender.com

■ REFERENCES

(1) Siddik, Z. H. Cisplatin: Mode of Cytotoxic Action and Molecular Basis of Resistance. *Oncogene* **2003**, *22*, 7265−7279.
(2) Galanski, M.; Jakupec, M.; Keppler, B. Update of the Preclinical Situation of Anticancer Platinum Complexes: Novel Design Strategies and Innovative Analytical Approaches. *Curr. Med. Chem.* **2005**, *12*, 2075−2094.
(3) Cepeda, V.; Fuertes, M. A.; Castilla, J.; Alonso, C.; Quevedo, C.; Perez, J. M. Biochemical Mechanisms of Cisplatin Cytotoxicity. *Anti-Cancer Agents Med. Chem.* **2007**, *7*, 3−18.
(4) Zajac, J.; Novohradsky, V.; Markova, L.; Brabec, V.; Kasparkova, J. Platinum (IV) Derivatives with Cinnamate Axial Ligands as Potent Agents Against Both Differentiated and Tumorigenic Cancer Stem Rhabdomyosarcoma Cells. *Angew. Chem., Int. Ed.* **2020**, *59*, 3329−3335.
(5) Yempala, T.; Babu, T.; Karmakar, S.; Nemirovski, A.; Ishan, M.; Gandin, V.; Gibson, D. Expanding the Arsenal of PtIV Anticancer Agents: Multi-Action PtIV Anticancer Agents with Bioactive Ligands Possessing a Hydroxy Functional Group. *Angew. Chem., Int. Ed.* **2019**, *58*, 18218−18223.
(6) Norman, D. J.; Gambardella, A.; Mount, A. R.; Murray, A. F.; Bradley, M. A Dual Killing Strategy: Photocatalytic Generation of Singlet Oxygen with Concomitant PtIV Prodrug Activation. *Angew. Chem., Int. Ed.* **2019**, *58*, 14189−14192.
(7) Babak, M. V.; Zhi, Y.; Czarny, B.; Toh, T. B.; Hooi, L.; Chow, E. K.-H.; Ang, W. H.; Gibson, D.; Pastorin, G. Dual-Targeting Dual-Action Platinum(IV) Platform for Enhanced Anticancer Activity and Reduced Nephrotoxicity. *Angew. Chem.* **2019**, *131*, 8193−8198.
(8) Ma, L.; Wang, N.; Ma, R.; Li, C.; Xu, Z.; Tse, M.-K.; Zhu, G. Monochalcoplatin: An Actively Transported, Quickly Reducible, and Highly Potent Pt IV Anticancer Prodrug. *Angew. Chem., Int. Ed.* **2018**, *57*, 9098−9102.
(9) Najjar, A.; Rajabi, N.; Karaman, R. Recent Approaches to Platinum(IV) Prodrugs: A Variety of Strategies for Enhanced Delivery and Efficacy. *Curr. Pharm. Des.* **2017**, *23*, 2366−2376.
(10) Ravera, M.; Gabano, E.; Zanellato, I.; Gallina, A.; Perin, E.; Arrais, A.; Cantamessa, S.; Osella, D. Cisplatin and Valproate Released from the Bifunctional $[Pt(IV)Cl_2(NH_3)_2(Valproato)_2]$ Antitumor Prodrug or from Liposome Formulations: Who Does What? *Dalton Trans.* **2017**, *46*, 1559−1566.
(11) Graf, N.; Lippard, S. J. Redox Activation of Metal-Based Prodrugs as a Strategy for Drug Delivery. *Adv. Drug Delivery Rev.* **2012**, *64*, 993−1004.
(12) Carr, J. L.; Tingle, M. D.; McKeage, M. J. Satraplatin Activation by Haemoglobin, Cytochrome C and Liver Microsomes in Vitro. *Cancer Chemother. Pharmacol.* **2006**, *57*, 483−490.
(13) Chaney, S. G.; Till, G. K.; Wyrick, S. In Vitro Biotransformations of Tetrachloro(d,l-Trans)-1,2-Diaminocyclohexaneplatinum(IV) (Tetraplatin) in Rat Plasma. *Cancer Res.* **1990**, *50*, 4539−4545.
(14) Gibbons, G. R.; Wyrick, S.; Chaney, S. G. Rapid Reduction of Tetrachloro(D,L-Trans)l,2-Diaminocyclohexaneplatinum(IV) (Tetraplatin) in RPMI 1640 Tissue Culture Medium. *Cancer Res.* **1989**, *49*, 1402−1407.
(15) Chen, C. K. J.; Zhang, J. Z.; Aitken, J. B.; Hambley, T. W. Influence of Equatorial and Axial Carboxylato Ligands on the Kinetic Inertness of Platinum(IV) Complexes in the Presence of Ascorbate and Cysteine and within DLD-1 Cancer Cells. *J. Med. Chem.* **2013**, *56*, 8757−8764.
(16) Kastner, A.; Poetsch, I.; Mayr, J.; Burda, J. V.; Roller, A.; Heffeter, P.; Keppler, B. K.; Kowol, C. R. A Dogma in Doubt: Hydrolysis of Equatorial Ligands of PtIV Complexes under Physiological Conditions. *Angew. Chem., Int. Ed.* **2019**, *58*, 7464−7469.
(17) Wexselblatt, E.; Raveendran, R.; Salameh, S.; Friedman-Ezra, A.; Yavin, E.; Gibson, D. On the Stability of PtIV Pro-Drugs with Haloacetato Ligands in the Axial Positions. *Chem. - Eur. J.* **2015**, *21*, 3108−3114.
(18) Gibson, D. Platinum (IV) Anticancer Prodrugs−Hypotheses and Facts. *Dalton Trans.* **2016**, *45*, 12983−12991.
(19) Li, Y.; Zhao, L.; Li, X. F. Targeting Hypoxia: Hypoxia-Activated Prodrugs in Cancer Therapy. *Front. Oncol.* **2021**, *11*, No. 700407.
(20) Sharma, A.; Arambula, J. F.; Koo, S.; Kumar, R.; Singh, H.; Sessler, J. L.; Kim, J. S. Hypoxia-targeted drug delivery. *Chem. Soc. Rev.* **2019**, *48*, 771−813.
(21) Ishiguro, T.; Ohata, H.; Sato, A.; Yamawaki, K.; Enomoto, T.; Okamoto, K. Tumor-Derived Spheroids: Relevance to Cancer Stem Cells and Clinical Applications. *Cancer Sci.* **2017**, *108*, 283−289.
(22) Xu, S.; Zhu, X.; Zhang, C.; Huang, W.; Zhou, Y.; Yan, D. Oxygen and Pt(II) Self-Generating Conjugate for Synergistic Photo-chemo Therapy of Hypoxic Tumor. *Nat. Commun.* **2018**, *9*, No. 2053.

(23) Guo, D.; Xu, S.; Yasen, W.; Zhang, C.; Shen, J.; Huang, Y.; Chen, D.; Zhu, X. Tirapazamine-Embedded Polyplatinum(Iv) Complex: A Prodrug Combo for Hypoxia-Activated Synergistic Chemotherapy. *Biomater. Sci.* **2020**, *8*, 694−701.
(24) Xu, Z.; Zhao, J.; Gou, S.; Xu, G. Novel Hypoxia-Targeting Pt(Iv) Prodrugs. *Chem. Commun.* **2017**, *53*, 3749−3752.
(25) Gabano, E.; Ravera, M.; Trivero, F.; Tinello, S.; Gallina, A.; Zanellato, I.; Gariboldi, M. B.; Monti, E.; Osella, D. The Cisplatin-Based Pt(Iv)-Diclorofibrato Multi-Action Anticancer Prodrug Exhibits Excellent Performances Also under Hypoxic Conditions. *Dalton Trans.* **2018**, *47*, 8268−8282.
(26) Cao, Q.; Zhou, D. J.; Pan, Z. Y.; Yang, G. G.; Zhang, H.; Ji, L. N.; Mao, Z. W. CAIXplatins: Highly Potent Platinum(IV) Prodrugs Selective Against Carbonic Anhydrase IX for the Treatment of Hypoxic Tumors. *Angew. Chem., Int. Ed.* **2020**, *59*, 18556−18562.
(27) Marland, J. R. K.; Gray, M. E.; Dunare, C.; Blair, E. O.; Tsiamis, A.; Sullivan, P.; González-Fernández, E.; Greenhalgh, S. N.; Gregson, R.; Clutton, R. E.; Parys, M. M.; Dyson, A.; Singer, M.; Kunkler, I. H.; Potter, M. A.; Mitra, S.; Terry, J. G.; Smith, S.; Mount, A. R.; Underwood, I.; Walton, A. J.; Argyle, D. J.; Murray, A. F. Real-Time Measurement of Tumour Hypoxia Using an Implantable Microfabricated Oxygen Sensor. *Sens. Bio-Sens. Res.* **2020**, *30*, No. 100375.
(28) Scigliano, S.; Pinel, S.; Poussier, S.; Fouyssac, F.; Plenat, F.; Karcher, G.; Chastagner, P. Measurement of Hypoxia Using Invasive Oxygen-Sensitive Electrode, Pimonidazole Binding and 18F-FDG Uptake in Anaemic or Erythropoietin-Treated Mice Bearing Human Glioma Xenografts. *Int. J. Oncol.* **2008**, *32*, 69−77.
(29) Hirata, K.; Yamaguchi, S.; Shiga, T.; Kuge, Y.; Tamaki, N. The Roles of Hypoxia Imaging Using18 F-Fluoromisonidazole Positron Emission Tomography in Glioma Treatment. *J. Clin. Med.* **2019**, *8*, No. 1088.
(30) Aguilera, K. Y.; Brekken, R. A. Hypoxia Studies with Pimonidazole in Vivo. *Bio-Protoc.* **2014**, *4*, No. e1254.
(31) Koch, C. J.; Evans, S. M.; Lord, E. M. Oxygen Dependence of Cellular Uptake of EF5 [2-(2-Nitro-1H-Imidazol-1-Yl)-N-(2, 2, 3, 3, 3-Pentafluoropropyl)a Cet Amide]: Analysis of Drug Adducts by Fluorescent Antibodies vs Bound Radioactivity. *Br. J. Cancer* **1995**, *72*, 869−874.
(32) Varghese, A. J.; Gulyas, S.; Mohindra, J. K. Hypoxia-dependent reduction of 1-(2-nitro-1-imidazolyl)-3-methoxy-2-propanol by Chinese Hamster Ovary cells and KHT tumor cells in vitro and in vivo. *Cancer Res.* **1976**, *36*, 3761−3765.
(33) Badar, S. B.; Zafar, K.; Ghafoor, R.; Khan, F. R. Comparative Evaluation of Chlorhexidine, Metronidazole and Combination Gels on Gingivitis: A Randomized Clinical Trial. *Int. J. Surg. Protoc.* **2019**, *14*, 30−33.
(34) Freeman, C. D.; Klutman, N. E.; Lamp, K. C. Metronidazole. A Therapeutic Review and Update. *Drugs* **1997**, *54*, 679−708.
(35) Nasirudeen, A. M. A.; Hian, Y. E.; Singh, M.; Tan, K. S. W. Metronidazole Induces Programmed Cell Death in the Protozoan Parasite Blastocystis Hominis. *Microbiology* **2004**, *150*, 33−43.
(36) Kawamoto, M.; Umebayashi, M.; Tanaka, H.; Koya, N.; Nakagawa, S.; Kawabe, K. E. N.; Onishi, H.; et al. Combined Gemcitabine and Metronidazole Is a Promising Therapeutic Strategy for Cancer Stem-like Cholangiocarcinoma. *Anticancer Res.* **2018**, *38*, 2739−2748.
(37) Yi, W.; Li, X.; He, X.; Yue, F.; Wang, T. Glass Nanopipette Sensing of Single Entities. *J. Electroanal. Chem.* **2022**, *909*, No. 116106.
(38) Bulbul, G.; Chaves, G.; Olivier, J.; Ozel, R.; Pourmand, N. Nanopipettes as Monitoring Probes for the Single Living Cell: State of the Art and Future Directions in Molecular Biology. *Cells* **2018**, *7*, No. 55.
(39) Wu, Y.; Shao, Y.; Zhang, W.; Li, B.; Zhao, L.; Zhang, D.; Guo, G.; Wang, X. Silica-Based Nanopipettes for Rapid Living Single-Cell Transfection. *ACS Appl. Nano Mater.* **2021**, *4*, 6956−6963.
(40) Wang, X.-Y.; Lv, J.; Hong, Q.; Zhou, Z.-R.; Li, D.-W.; Qian, R.-C. Nanopipette-Based Nanosensor for Label-Free Electrochemical Monitoring of Cell Membrane Rupture under H_2O_2 Treatment. *Anal. Chem.* **2021**, *93*, 13967−13973.
(41) Yu, R.; Ying, Y.; Gao, R.; Long, Y. Confined Nanopipette Sensing: From Single Molecules, Single Nanoparticles, to Single Cells. *Angew. Chem., Int. Ed.* **2019**, *58*, 3706−3714.
(42) Zhang, X.-W.; Oleinick, A.; Jiang, H.; Liao, Q.-L.; Qiu, Q.-F.; Svir, I.; Liu, Y.-L.; Amatore, C.; Huang, W.-H. Electrochemical Monitoring of ROS/RNS Homeostasis Within Individual Phagolysosomes Inside Single Macrophages. *Angew. Chem., Int. Ed.* **2019**, *58*, 7753−7756.
(43) Wang, Y.; Noël, J. M.; Velmurugan, J.; Nogala, W.; Mirkin, M. V.; Lu, C.; Collignon, M. G.; Lemaître, F.; Amatore, C. Nanoelectrodes for Determination of Reactive Oxygen and Nitrogen Species inside Murine Macrophages. *Proc. Natl. Acad. Sci. U.S.A.* **2012**, *109*, 11534−11539.
(44) Hu, K.; Li, Y.; Rotenberg, S. A.; Amatore, C.; Mirkin, M. V. Electrochemical Measurements of Reactive Oxygen and Nitrogen Species inside Single Phagolysosomes of Living Macrophages. *J. Am. Chem. Soc.* **2019**, *141*, 4564−4568.
(45) Li, Y.; Hu, K.; Yu, Y.; Rotenberg, S. A.; Amatore, C.; Mirkin, M. V. Direct Electrochemical Measurements of Reactive Oxygen and Nitrogen Species in Nontransformed and Metastatic Human Breast Cells. *J. Am. Chem. Soc.* **2017**, *139*, 13055−13062.
(46) Zhang, X.; Hatamie, A.; Ewing, A. G. Nanoelectrochemical Analysis inside a Single Living Cell. *Curr. Opin. Electrochem.* **2020**, *22*, 94−101.
(47) Actis, P.; Tokar, S.; Clausmeyer, J.; Babakinejad, B.; Mikhaleva, S.; Cornut, R.; Takahashi, Y.; López Córdoba, A.; Novak, P.; Shevchuck, A. I.; Dougan, J. A.; Kazarian, S. G.; Gorelkin, P. V.; Erofeev, A. S.; Yaminsky, I. V.; Unwin, P. R.; Schuhmann, W.; Klenerman, D.; Rusakov, D. A.; Sviderskaya, E. V.; Korchev, Y. E. Electrochemical Nanoprobes for Single-Cell Analysis. *ACS Nano* **2014**, *8*, 875−884.
(48) Erofeev, A.; Gorelkin, P.; Garanina, A.; Alova, A.; Efremova, M.; Vorobyeva, N.; Edwards, C.; Korchev, Y.; Majouga, A. Novel Method for Rapid Toxicity Screening of Magnetic Nanoparticles. *Sci. Rep.* **2018**, *8*, No. 7462.
(49) Akasov, R. A.; Sholina, N. V.; Khochenkov, D. A.; Alova, A. V.; Gorelkin, P. V.; Erofeev, A. S.; Generalova, A. N.; Khaydukov, E. V. Photodynamic Therapy of Melanoma by Blue-Light Photoactivation of Flavin Mononucleotide. *Sci. Rep.* **2019**, *9*, No. 9679.
(50) Krasnovskaya, O. O.; Guk, D. A.; Naumov, A. E.; Nikitina, V. N.; Semkina, A. S.; Vlasova, K. Y.; Pokrovsky, V.; Ryabaya, O. O.; Karshieva, S. S.; Skvortsov, D. A.; Zhirkina, I. V.; Shafikov, R. R.; Gorelkin, P. V.; Vaneev, A. N.; Erofeev, A. S.; Mazur, D. M.; Tafeenko, V. A.; Pergushov, V. I.; Melnikov, M. Y.; Soldatov, M. A.; Shapovalov, V. V.; Soldatov, A. V.; Akasov, R. A.; Gerasimov, V. M.; Sakharov, D. A.; Moiseeva, A. A.; Zyk, N. V.; Beloglazkina, E. K.; Majouga, A. G. Novel Copper-Containing Cytotoxic Agents Based on 2-Thioxoimidazolones. *J. Med. Chem.* **2020**, *63*, 13031−13063.
(51) Vaneev, A. N.; Gorelkin, P. V.; Garanina, A. S.; Lopatukhina, H. V.; Vodopyanov, S. S.; Alova, A. V.; Ryabaya, O. O.; Akasov, R. A.; Zhang, Y.; Novak, P.; Salikhov, S. V.; Abakumov, M. A.; Takahashi, Y.; Edwards, C. R. W.; Klyachko, N. L.; Majouga, A. G.; Korchev, Y. E.; Erofeev, A. S. In Vitro and In Vivo Electrochemical Measurement of Reactive Oxygen Species After Treatment with Anticancer Drugs. *Anal. Chem.* **2020**, *92*, 8010−8014.
(52) Vaneev, A. N.; Gorelkin, P. V.; Krasnovskaya, O. O.; Akasov, R. A.; Spector, D. V.; Lopatukhina, E. V.; Timoshenko, R. V.; Garanina, A. S.; Zhang, Y.; Salikhov, S. V.; Edwards, C. R. W.; Klyachko, N. L.; Takahashi, Y.; Majouga, A. G.; Korchev, Y. E.; Erofeev, A. S. In Vitro / In Vivo Electrochemical Detection of Pt(II) Species. *Anal. Chem.* **2022**, *94*, 4901−4905.
(53) Spector, D. V.; Pavlov, K. G.; Akasov, R. A.; Vaneev, A. N.; Erofeev, A. S.; Gorelkin, P. V.; Nikitina, V. N.; Lopatukhina, E. V.; Semkina, A. S.; Vlasova, K. Y.; Skvortsov, D. A.; Roznyatovsky, V. A.; Ul, N. V.; Pikovskoi, I. I.; Sypalov, S. A.; Garanina, A. S.; Vodopyanov, S. S.; Abakumov, M. A.; Volodina, Y. L.; Markova, A. A.; Petrova, A. S.; Mazur, D. M.; Sakharov, D. A.; Zyk, N. V.; Beloglazkina, E. K.;

https://doi.org/10.1021/acs.inorgchem.2c02062
Inorg. Chem. 2022, 61, 14705−14717

Majouga, A. G.; Krasnovskaya, O. O. Pt(IV) Prodrugs with Non-Steroidal Anti-in Fl Ammatory Drugs in the Axial Position. *J. Med. Chem.* **2022**, *65*, 8227−8244.
(54) Pathak, R. K.; Marrache, S.; Choi, J. H.; Berding, T. B.; Dhar, S. The Prodrug Platin-A: Simultaneous Release of Cisplatin and Aspirin. *Angew. Chem., Int. Ed.* **2014**, *53*, 1963−1967.
(55) Mura, C.; Valenti, D.; Floris, C.; Sanna, R.; De Luca, M. A.; Fadda, A. M.; Loy, G. Metronidazole Prodrugs: Synthesis, Physicochemical Properties, Stability, and Ex Vivo Release Studies. *Eur. J. Med. Chem.* **2011**, *46*, 4142−4150.
(56) Dittert, L. W.; Caldwell, H. C.; Adams, H. J.; Irwin, G. M.; Swintosky, J. V. Acetaminophen Prodrugs I. Synthesis, Physicochemical Properties, and Analgesic Activity. *J. Pharm. Sci.* **1968**, *57*, 774−780.
(57) Tolan, D.; Gandin, V.; Morrison, L.; El-Nahas, A.; Marzano, C.; Montagner, D.; Erxleben, A. Oxidative Stress Induced By Pt(IV) Pro-Drugs Based On The Cisplatin Scaffold And Indole Carboxylic Acids In Axial Position. *Sci. Rep.* **2016**, *6*, No. 29367.
(58) Zhang, J. Z.; Wexselblatt, E.; Hambley, T. W.; Gibson, D. Pt(IV) Analogs Of Oxaliplatin That Do Not Follow The Expected Correlation Between Electrochemical Reduction Potential And Rate Of Reduction By Ascorbate. *Chem. Commun.* **2012**, *48*, 847−849.
(59) Luo, X.; Gong, X.; Su, L.; Lin, H.; Yang, Z.; Yan, X.; Gao, J. Activatable Mitochondria-Targeting Organoarsenic Prodrugs for Bioenergetic Cancer Therapy. *Angew. Chem., Int. Ed.* **2021**, *60*, 1403−1410.
(60) Kleih, M.; Böpple, K.; Dong, M.; Gaißler, A.; Heine, S.; Olayioye, M. A.; Aulitzky, W. E.; Essmann, F. Direct Impact of Cisplatin on Mitochondria Induces ROS Production That Dictates Cell Fate of Ovarian Cancer Cells. *Cell Death Dis.* **2019**, *10*, No. 851.
(61) Cocetta, V.; Ragazzi, E.; Montopoli, M. Mitochondrial Involvement in Cisplatin Resistance. *Int. J. Mol. Sci.* **2019**, *20*, No. 3384.
(62) Marrache, S.; Pathak, R. K.; Dhar, S. Detouring of Cisplatin to Access Mitochondrial Genome for Overcoming Resistance. *Proc. Natl. Acad. Sci. U.S.A.* **2014**, *111*, 10444−10449.
(63) Jin, S.; Hao, Y.; Zhu, Z.; Muhammad, N.; Zhang, Z.; Wang, K.; Guo, Y.; Guo, Z.; Wang, X. Impact of Mitochondrion-Targeting Group on the Reactivity and Cytostatic Pathway of Platinum(IV) Complexes. *Inorg. Chem.* **2018**, *57*, 11135−11145.
(64) Hall, M. D.; Foran, G. J.; Zhang, M.; Beale, P. J.; Hambley, T. W. XANES Determination of the Platinum Oxidation State Distribution in Cancer Cells Treated with Platinum(IV) Anticancer Agents. *J. Am. Chem. Soc.* **2003**, *125*, 7524−7525.
(65) Hall, M. D.; Daly, H. L.; Zhang, J. Z.; Zhang, M.; Alderden, R. A.; Pursche, D.; Foran, G. J.; Hambley, T. W. Quantitative Measurement of the Reduction of Platinum(IV) Complexes Using X-Ray Absorption near-Edge Spectroscopy (XANES). *Metallomics* **2012**, *4*, 568−575.
(66) Bolitho, E. M.; Sanchez-Cano, C.; Shi, H.; Quinn, P. D.; Harkiolaki, M.; Imberti, C.; Sadler, P. J. Single-Cell Chemistry of Photoactivatable Platinum Anticancer Complexes. *J. Am. Chem. Soc.* **2021**, *143*, 20224−20240.
(67) Chen, C. K. J.; Kappen, P.; Gibson, D.; Hambley, T. W. transPlatinum(IV) prodrugs that exhibit unusual resistance to reduction by endogenous reductants and blood serum but are rapidly activated inside cells: 1H NMR and XANES spectroscopy study. *Dalton Trans.* **2020**, *49*, 7722−7736.
(68) Chen, C. K. J.; Kappen, P.; Hambley, T. W. The Reduction of: Cis -Platinum(Iv) Complexes by Ascorbate and in Whole Human Blood Models Using 1 H NMR and XANES Spectroscopy. *Metallomics* **2019**, *11*, 686−695.
(69) Nemirovski, A.; Kasherman, Y.; Tzaraf, Y.; Gibson, D. Reduction of Cis,Trans,Cis-[PtCl2(OCOCH3)2(NH3)2] by Aqueous Extracts of Cancer Cells. *J. Med. Chem.* **2007**, *50*, 5554−5556.
(70) Nemirovski, A.; Vinograd, I.; Takrouri, K.; Mijovilovich, A.; Rompel, A.; Gibson, D. New Reduction Pathways for Ctc-[PtCl2-(CH3CO 2)2(NH3)(Am)] Anticancer Prodrugs. *Chem. Commun.* **2010**, *46*, 1842−1844.
(71) Krasnovskaya, O.; Spector, D.; Erofeev, A.; Gorelkin, P.; Akasov, R.; Skvortsov, D.; Trigub, A.; Vlasova, K.; Semkina, A.; Zyk, N.; Beloglazkina, E.; Majouga, A. Alternative Mechanism Of Action Of The DNP Ptivprodrug: Intracellular Cisplatin Release And The Mitochondria-Mediated Apoptotic Pathway. *Dalton Trans.* **2021**, *50*, 7922−7927.
(72) Zhang, J. Z.; Wexselblatt, E.; Hambley, T. W.; Gibson, D. Pt(Iv) Analogs of Oxaliplatin That Do Not Follow the Expected C orrelation between Electrochemical Reduction Potential and Rate of Reduction by Ascorbate. *Chem. Commun.* **2012**, *48*, 847−849.
(73) Ellis, L. T.; Er, H. M.; Hambley, T. W. The Influence of the Axial Ligands of a Series of Platinum(Iv) Anti-Cancer Complexes on Their Reduction to Platinum(II) and Reaction with DNA. *Aust. J. Chem.* **1995**, *48*, 793−806.
(74) Choi, S.; Filotto, C.; Bisanzo, M.; Delaney, S.; Lagasee, D.; Whitworth, J. L.; Jusko, A.; Li, C.; Wood, N. A.; Willingham, J.; Schwenker, A.; Spaulding, K. Reduction and Anticancer Activity of Platinum(IV) Complexes. *Inorg. Chem.* **1998**, *37*, 2500−2504.
(75) Nunes, A. S.; Barros, A. S.; Costa, E. C.; Moreira, A. F.; Correia, I. J. 3D Tumor Spheroids as in Vitro Models to Mimic in Vivo Human Solid Tumors Resistance to Therapeutic Drugs. *Biotechnol. Bioeng.* **2019**, *116*, 206−226.
(76) Millard, M.; Yakavets, I.; Zorin, V.; Kulmukhamedova, A.; Marchal, S.; Bezdetnaya, L. Drug Delivery to Solid Tumors: The Predictive Value of the Multicellular Tumor Spheroid Model for Nanomedicine Screening. *Int. J. Nanomed.* **2017**, *12*, 7993−8007.
(77) Ham, S. L.; Joshi, R.; Luker, G. D.; Tavana, H. Engineered Breast Cancer Cell Spheroids Reproduce Biologic Properties of Solid Tumors. *Adv. Healthcare Mater.* **2016**, *5*, 2788−2798.
(78) Ito, M.; Yang, D. J.; Mawlawi, O.; Mendez, R.; Oh, C. S.; Azhdarinia, A.; Greenwell, A. C.; Yu, D. F.; Kim, E. E. PET and Planar Imaging of Tumor Hypoxia With Labeled Metronidazole. *Acad. Radiol.* **2006**, *13*, 598−609.
(79) Löfmark, S.; Edlund, C.; Nord, C. E. Metronidazole Is Still the Drug of Choice for Treatment of Anaerobic Infections. *Clin. Infect. Dis.* **2010**, *50*, S16−S23.
(80) Alova, A.; Erofeev, A.; Gorelkin, P.; Bibikova, T.; Korchev, Y.; Majouga, A.; Bulychev, A. Prolonged Oxygen Depletion in Micro-wounded Cells of Chara Corallina Detected with Novel Oxygen Nanosensors. *J. Exp. Bot.* **2020**, *71*, 386−398.
(81) Edwards, D. I. Reduction of Nitroimidazoles in Vitro and DNA Damage. *Biochem. Pharmacol.* **1986**, *35*, 53−58.
(82) Yalikun, N.; Mamat, X.; Li, Y.; Hu, X.; Wang, P.; Hu, G. N, S, P-Triple Doped Porous Carbon as an Improved Electrochemical Sensor for Metronidazole Determination. *J. Electrochem. Soc.* **2019**, *166*, B1131−B1137.
(83) Nikodimos, Y.; Amare, M. Electrochemical Determination of Metronidazole in Tablet Samples Using Carbon Paste Electrode. *J. Anal. Methods Chem.* **2016**, *2016*, 1−7.
(84) Gopi, P. K.; Kesavan, G.; Chen, S. M.; Ravikumar, C. H. Cadmium Sulfide Quantum Dots Anchored on Reduced Graphene Oxide for the Electrochemical Detection of Metronidazole. *New J. Chem.* **2021**, *45*, 3022−3033.
(85) Shen, C.; Harris, B. D. W.; Dawson, L. J.; Charles, K. A.; Hambley, T. W.; New, E. J. Fluorescent Sensing Of Monofunctional Platinum Species. *Chem. Commun.* **2015**, *51*, 6312−6314.
(86) Laviron, E. General Expression of the Linear Potential Sweep Voltammogram in the Case of Diffusionless Electrochemical Systems. *J. Electroanal. Chem. Interfacial Electrochem.* **1979**, *101*, 19−28.
(87) Grimes, D. R.; Kelly, C.; Bloch, K.; Partridge, M. A Method for Estimating the Oxygen Consumption Rate in Multicellular Tumour Spheroids. *J. R. Soc., Interface* **2014**, *11*, No. 20131124.
(88) Ryabaya, O.; Prokofieva, A.; Akasov, R.; Khochenkov, D.; Emelyanova, M.; Burov, S.; Markvicheva, E.; Inshakov, A.; Stepanova, E. Metformin Increases Antitumor Activity of MEK Inhibitor Binimetinib in 2D and 3D Models of Human Metastatic Melanoma Cells. *Biomed. Pharmacother.* **2019**, *109*, 2548−2560.

https://doi.org/10.1021/acs.inorgchem.2c02062
Inorg. Chem. 2022, 61, 14705−14717